

University of New Hampshire

University of New Hampshire Scholars' Repository

Master's Theses and Capstones

Student Scholarship

Winter 2022

DESIGN AND SYNTHESIS TOWARDS BIFUNCTIONAL 89ZR AND 44SC CHELATORS FOR IMMUNO-POSITRON EMISSION TOMOGRAPHY

Noah Cote

University of New Hampshire, Durham

Follow this and additional works at: <https://scholars.unh.edu/thesis>

Recommended Citation

Cote, Noah, "DESIGN AND SYNTHESIS TOWARDS BIFUNCTIONAL 89ZR AND 44SC CHELATORS FOR IMMUNO-POSITRON EMISSION TOMOGRAPHY" (2022). *Master's Theses and Capstones*. 1642.
<https://scholars.unh.edu/thesis/1642>

This Thesis is brought to you for free and open access by the Student Scholarship at University of New Hampshire Scholars' Repository. It has been accepted for inclusion in Master's Theses and Capstones by an authorized administrator of University of New Hampshire Scholars' Repository. For more information, please contact Scholarly.Communication@unh.edu.

DESIGN AND SYNTHESIS TOWARDS BIFUNCTIONAL ^{89}Zr AND ^{44}Sc CHELATORS
FOR IMMUNO-POSITRON EMISSION TOMOGRAPHY

BY

NOAH A. COTE

B.S. University of New Hampshire, 2019

MASTERS THESIS

Submitted to University of New Hampshire

in Partial Fulfillment of

the Requirements for the Degree of

Master of Science

In

Chemistry

December 2022

This thesis was examined and approved in partial fulfillment of the requirement for the degree of
Master of Science in Chemistry by:

Thesis Director, Roy Planalp,
Associate Professor of Chemistry

Erik B. Berda,
Department Chair and Professor of Chemistry

Nathan J. Oldenhuis,
Assistant Professor of Chemistry

On 12/16/2022

Original approval signatures are on file with the University of New Hampshire Graduate School.

DEDICATION

I dedicate this thesis to my father Alan. My dad has been my inspiration since day one and I'm glad that I will be able to prove to him all the hard work and dedication I've put into my work. He has always pushed me to be the best version of myself as possible, and if not for that I wouldn't be where I am today.

ACKNOWLEDGEMENTS

Firstly, I would like to thank my advisor Dr. Roy Planalp. Without his help, I may have faltered one too many times during my career as a graduate student. When possible, he would show me the errors of my way in and outside of the lab, leading me to many of my successes. I would also like to extend my thanks to my thesis committee consisting of Dr. Erik Berda and Dr. Nathan Oldenhuis for taking the time to read this document.

The next thanks go out to my fellow research group members and others I shared an office with. Ryan has aided me throughout most of my research career as an undergraduate as well as a graduate student. Ryan and Leo give me the day to day support I needed to make it as a synthetic chemist. Furthermore, other members of our office including Nick and Taylir became lifelong friends, and I couldn't be here without them.

Other thanks go out to Cindi Rohwer, Laura Bicknell, Kristen Blackwell, Marjorie Williams, Svetlana Shuba, and Dr. Patricia Stone. This team is integral to the success of any graduate student and any assistance has been greatly appreciated.

TABLE OF CONTENTS

DEDICATION.....	iii
ACKNOWLEDGEMENTS.....	iv
LIST OF SCHEMES.....	vii
LIST OF FIGURES.....	viii
ABSTRACT.....	x

GENERAL INTRODUCTION.....	1
---------------------------	---

CHAPTER	PAGE
I. COMPUTATIONAL ANALYSIS OF AND SYNTHETIC PROGRESS TOWARDS BIFUNCTIONAL NITROGEN BASED MACROCYCLES FOR IMMUNO-PET.....	8
A. Ligand Design for Sc-Based Radiotherapeutics.....	8
B. N-Based Macrocycles and Derivatives.....	9
C. Computational Design of Phosphinate N-Based Macrocycles.....	9
D. Computational Results.....	14
E. Synthesis of Bifunctional Sc ³⁺ Chelator for ImmunoPET.....	18
F. Conclusions and Future Work.....	25
II. DESIGN AND SYNTHETIC PROGRESS TOWARDS A NOVEL BIFUNCTIONAL CHELATOR FOR ⁸⁹ ZR AND IMMUNO-PET.....	26
A. Ligand Design for Zr-Based Radiotherapeutics.....	26
B. Deferoxamine B (DFO).....	27
C. Synthesis of Bifunctional Zr ⁴⁺ Chelator.....	28

D. Conclusions and Future Work.....	31
III. EXPERIMENTAL SECTION.....	32
A. General Methods.....	32
B. Detailed Experimental.....	33
LIST OF REFERENCES.....	44
APPENDIX.....	49

LIST OF SCHEMES

NUMBER	PAGE
1. Synthetic design of bifunctional complex (17) $\text{Sc}^{\text{III}}(\text{p-NO}_2\text{-Bn-NOTPi})$	14
2. Synthetic design of model complex (20) $\text{Sc}^{\text{III}}(\text{NOTPi})$	14
3. Synthesis of bifunctional complex (24) $\text{Zr}^{\text{IV}}(\text{p-NO}_2\text{-Sal-DFO})$	29

LIST OF FIGURES

NUMBER	PAGE
1-1. Structure of bifunctional triazamacrocyclic complex (17).....	10
1-2. Structures of DOTA (left), DOTP (middle), and DOTPi (right).....	11
1-3. Structure of derived DOTPi and functionalized NOTPi.....	12
1-4. Structures of Zr^{4+} (DOTA) [left], Zr^{4+} (DOTP) [middle], and Zr^{4+} (DOTPi) [right].....	13
1-5. Key bond lengths calculated for Zr^{4+} (DOTA), Zr^{4+} (DOTP), and Zr^{4+} (DOTPi).....	15
1-6. Structures of $[Zr^{4+}(\text{DOTA})(\text{H}_2\text{O})]$ {left}, $[Zr^{4+}(\text{DOTP})(\text{H}_2\text{O})]$ {middle}, and $[Zr^{4+}(\text{DOTPi})(\text{H}_2\text{O})]$ {left}	16
1-7. Key bond lengths calculated for $[Zr^{4+}(\text{DOTA})(\text{H}_2\text{O})]$, $[Zr^{4+}(\text{DOTP})(\text{H}_2\text{O})]$, and $[Zr^{4+}(\text{DOTPi})(\text{H}_2\text{O})]$	17
1-8. Nitration of L-Phenylalanine.....	18
1-9. ^1H NMR of 4-nitro-phenylalanine.....	18
1-10. Formation of methyl ester via SOCl_2	19
1-11. Formation of amide.....	19
1-12. Formation of diamine dihydrochloride salt.....	20
1-13. Formation of ditosyl diamine.....	20
1-14. Formation of tritosyl diethanolamine.....	21
1-15. Attempted cyclization to p-NO ₂ -Bn-Tritosyl TACN.....	22
1-16. Formation of ditosyl ethylenediamine.....	22
1-17. Richman-Atkins cyclization to tritosyl TACN.....	23
1-18. Formation of TACN.....	24
1-19. Attempted formation of phosphinate derivative of TACN.....	25

2-1.	Structures of DFO (top), DTPA (left), EDTA (right), and DOTA (bottom).....	31
2-2.	Synthesis of active ester.....	32
2-3.	Functionalization of DFO-NH ₂	33
2-4.	TOF ESI-MS of functionalized DFO.....	34
2-5.	Synthesis of Zr ^{IV} (AHA).....	34

ABSTRACT

DESIGN AND SYNTHESIS OF BIFUNCTIONAL ^{89}Zr AND ^{44}Sc CHELATORS FOR IMMUNO-POSITRON EMISSION TOMOGRAPHY

By

Noah Alan Cote

University of New Hampshire, December 2022

The design and synthesis of novel zirconium and scandium complexes, $\text{Zr}^{\text{IV}}(\text{p-NO}_2\text{-sal-DFO})$ and $\text{Sc}^{\text{III}}(\text{p-NO}_2\text{-Bn-NOTPi})$ respectively, and their potential for use in immuno-positron emission tomography (immuno-PET) are discussed. The design for a linear octadentate ligand for Zr was hypothesized and derived from deferoxamine B (DFO), a well-known hexadentate siderophore for Fe complexation. A p-NO₂-salicylic acid derivative was prepared to provide a bifunctional handle for antibody conjugation. Deferoxamine B chelates with hydroxamate moieties, which have proven useful for chelation of hard acids. While difficulties in purification led to no complexation studies being performed, this chelator was confirmed via ^1H NMR, ^{13}C NMR, and time-of-flight electron ionization mass spectrometry (TOF ESI-MS). A cyclic hexadentate ligand for Sc derived from 1,4,7-triazacyclononane (TACN) was chosen because it can be readily derived. The design and viability for this ligand has been worked on computationally using a model cyclic, octadentate chelator derived from 1,4,7,10-

tetraazacyclododecane (cyclen). This work led to design and undertaking of a multistep synthesis to the novel complex, $\text{Sc}^{\text{III}}(\text{p-NO}_2\text{-Bn-NOTPi})$, which incorporates phosphinate pendant arms and a para-nitrobenzyl group for bioconjugation. While the synthesis of p-NO₂-Bn-NOTPi has not been completed, intermediates have been analyzed via ¹H NMR, ¹³C NMR.

INTRODUCTION

With cancer detection becoming a more prevalent necessity within today's society, advances in therapeutic diagnostics have paved the way for new techniques and possibilities to aid these hardships. One such technique is positron emission tomography (PET), a 3-D nuclear imaging technique one can use to monitor changes in metabolic behavior.¹⁻⁵ Using radiotracers, one can monitor processes such as blood flow, local composition, or even detect cancers. The use of radiolabeled antibodies is also a process which has been used in clinical diagnostic for over 50 years.¹⁻³ When used in combination with PET, a technique known as immuno-PET is born. This non-invasive technique has shown to be an effective tumor detection strategy because it combines the high sensitivity of PET with radiolabeled antibodies' high specificity.⁴ Since its birth, immuno-PET has drastically increased the availability of tumor detection agents and has sprung to the forefront of medical science as we know it today.

As stated, PET is a 3-D nuclear imaging technique that relies on the decay of radiotracers. While PET can be performed as a 2-D technique, there are advantages when applied as a 3-D image. 3-D imaging allows for a significantly increased count rate per scan, while increasing the number of random events, drastically increases the number of desired events. As a result of increased desired events, overall scan time for a full body PET scan decreases and therefore radiation dosage to patients also decreases. This is a significant advantage over another imaging technique known as SPECT (single-photon emission computerized technology). SPECT scans result in 2-D images that are then reconstructed into a 3-D data set. Another advantage of PET vs. SPECT is the drastically increased sensitivity due to coincident detection. Coincident

detection allows for proper 3-D images to be made with highly improved sensitivity and improved image quality with shorter scan times when compared to SPECT.⁶³

When radiotracers decay there is an emission of a high-energy particle known as positron, the antiparticle to the electron. The positron will then lose kinetic energy as it travels through tissue, and eventually encounter an electron. When this occurs an incredibly short-lived positronium ion will form and then immediately annihilate into equivalent gamma photons that travel in opposite directions. The emission of annihilated gamma photons in opposite directions allows PET to give 3-D images. When gamma photons are released, they travel and eventually contact a scintillator; this creates a short burst of light that can be detected when in conjunction with a photomultiplier tube. If the detection of the pair of gamma photons does not occur within a few nanoseconds, it is ignored because localization of the annihilation event becomes difficult and image reconstruction becomes impossible. This style of detection, known as coincident detection, comes with significant flaws because several aspects can lead to weak signal to noise. Such causes of noise include the simultaneous detection of gamma photons that were produced from different annihilation events. Even though there are parameters than can correct for this, PET remains difficult in practice and requires tremendous care when performing such procedures.⁵

Selection of Radiotracers

Many isotopes perform the necessary nuclear decay for immuno-PET application, but most have flaws preventing them from being useful in imaging applications. For years the field was dominated by ¹⁸F labeled agents due to its adequate half-life and relative ease of production.^{1-4,13} While this has been an effective radiotracer, the half-life of 1.92 hours does limit

the use of ^{18}F to mainly on-site use. For this reason, many other radionuclides have been studied that challenge the use of ^{18}F of which include: ^{68}Ga , ^{64}Cu , ^{89}Zr , and ^{44}Sc . ^{68}Ga has been an attractive radio tracer due to its availability of production through $^{68}\text{Ge}/^{68}\text{Ga}$ generator and quality imaging but also falters due to inherent high cost and a half-life of only 68 minutes.^{14,15} ^{64}Cu on the other hand has an impressive 12.7-hour half-life allowing for much more flexible radiochemistry to be performed, but weak signal requiring high dosage amount for clinical studies.¹⁶

^{44}Sc includes both advantages of ^{68}Ga and ^{64}Cu with an impressive signal to dosage ratio and a half-life of 3.97 hours. This allows for a wide variety chemistry to be performed before the effective radiative decay wears off.¹⁷⁻²⁰ As of 2014 there are two main ways to generate the scandium isotope: $^{44}\text{Ti}/^{44}\text{Sc}$ generators, and cyclotron irradiation of ^{44}Ca .^{21,22} To date, the cyclotron irradiation of either natural or ^{44}Ca enriched targets has proven to be the most cost-efficient mean of ^{44}Sc production. The decay of ^{44}Sc into ^{44}Ca can be an issue as this radioisotope can linger in the body if not properly complexed. This damage may be lesser than other radioisotopes since the body has a natural use for calcium within teeth and bones.⁶⁴

One highly desirable trait of ^{89}Zr is the half-life of 3.3 days, which makes ^{89}Zr a very suitable isotope for immunoPET, consistent with the pharmacokinetics of many monoclonal antibodies (mABs).⁵²⁻⁵⁴ Also the means of production for this isotope has proven to be rather simple. ^{89}Zr is easily produced as shown by Link et al. via proton irradiation of abundant, naturally occurring ^{89}Y , which afforded the neutron deficient isotope ^{89}Zr . After several purification steps this method provided an 80% yield and >99% radionuclidic purity.⁵⁵ The ^{89}Zr isotope is now made by cyclotron bombardment of ^{89}Y foils, which is economical relative to other isotope preparations.⁵⁶ While the means of production and decay process is desirable, ^{89}Zr

decays to ^{89}Y which is a strong gamma-emitter. The energy of decay and different chemical properties of ^{89}Y cause decomplexation or damage to the chelator and free $^{89}\text{Y}^{3+}$ can then remain in the kidneys, bladder, or bone marrow.⁵⁷⁻⁶²

The use of radioactive metals in medicinal chemistry leads to a fine balance between proper half-life selection and risk of acquired health conditions. This document will discuss the use of both Zr and Sc as potential radiotracers for immuno-PET.

Design of Chelators

To aid in the potential health concerns of using certain longer-lived isotopes, proper chelator design is vital. When designing a chelator, several factors need to be considered: ring size, hard/soft acid/base theory, and proper coordination denticity. If these conditions are not met the strength of chelation will be poor and the complex may fall apart, leading to the potential for deposits to occur as discussed above. We have focused on radioisotopes ^{89}Zr and ^{44}Sc and proper chelator design becomes essential to limit decomplexation and subsequent deposition of unwanted, harmful materials.

Firstly, within our design the use of ligands that fall into the correct hard/soft acid/base (HSAB) theory or otherwise known as Pearson's acid base concept.⁶ Hard bases include elements such as N, O, and F due to their small size and nature of polarizability. Generally, nitrogen is considered a borderline base and can coordinate hard and soft acids. The metals being coordinated are that of group 3 and 4 d-block elements and therefore fall into the classification of hard acids. Hard acids generally are small and contain greater charge density.⁶ Sc^{III} and Zr^{IV} have ionic radii of 88.5 pm and 98 pm in their preferred coordination number. Combining this with their high charge density, these metals fall well into the classification of hard acids.⁷⁻⁸ The design

for a linear Zr^{IV} chelator was derived from deferoxamine B (DFO) which can coordinate metals through its three hydroxamic acid (OCNO) moieties. Hydroxamic acids coordinate metals through two oxygen species, making DFO a strong chelator of hard acids such as Fe³⁺.⁹ The design for a Sc^{III} chelator is derived from the nitrogen-based macrocycle TACN, which will be N-functionalized with three pendant phosphinate arms. This will lead to a six-coordinate complex comprised of three oxygen chelates and three nitrogen chelates. Conditions such as these should be appropriate for hard acid species such as Sc^{III}.

Ring size is also an important factor when designing coordination complexes. It has been proven that metals of larger ionic radii prefer five-membered chelate rings and metals of smaller ionic radii prefer six-membered chelate rings.⁸ Sc^{III} and Zr^{IV} are early group d-block elements, and are larger in size compared to other metal ions with the same oxidation state.⁷ The preference for either five or six membered rings comes from the angle strain within the chelate ring. Larger ions prefer five-membered rings because the angle strain is weaker due to the bond angles being larger. Inversely, smaller ions can allow for the angle strain of a six-membered ring.⁸ In this work the hydroxamic acid moiety for Zr complexation, and N-functionalized phosphinate moieties for Sc complexation result in five-membered chelate rings.

Computational Chemistry

In this work, computational analysis of Zr tetraazamacrocycles was performed. The geometries were optimized using density functional theory (DFT), a quantum mechanical modelling method. Using this method, one can accurately depict the electron density of atoms and molecules and reconstruct an appropriate structure based on the input provided.

Depending on the elements being computed, different basis sets within the B3LYP functional may be required.^{10,11} The Becke, 3-parameter, Lee–Yang–Parr B3LYP functional has become a widely used functional when computing equilibrium geometries of molecules. Using the electronic wave function, these functionals turn the partial differential equations provided by the model to algebraic equations that can be computed by the software. In general, first row organic elements such as H, C, N, and O can be depicted with relative accuracy using the 6-31g* basis set. Breaking this down, each inner shell basis function is a sum of 6 Gaussians, and each valence basis function is split into inner and outer parts comprising of three and one Gaussians, respectively. The * notation represents changes in hybridization of the orbitals. One * applies d-orbital character to p-orbitals while two ** applies p-orbital character to s-orbitals.¹² Other heavier atoms, such as Zr discussed in this work, require an effective-core potential basis set or pseudopotential.^{10,11} This type of basis set assumes inner shell electron density and focuses on computing more valence shell electron density. This helps ease the computational load on the computer and accurately depicts the valence shells of heavier metal atoms. In our computations for elements C, H, N, and O the 6-31g* basis set was used; for P the 6-311g** basis set was used; and for Zr the Los Alamos National Laboratory 2-double-z (LANL2DZ) pseudopotential basis set was used.

Traditionally ¹⁸F is used for PET, and many pre- and post-clinical trials have been successful.¹⁻⁴ Over more recent years, radioisotopes ⁸⁹Zr and ⁴⁴Sc have been of significant interest due to their increased half-lives, 78.26 hours, and 4.04 hours, respectively. Comparatively, ¹⁸F has a half-life of 1.92 hr.¹⁻⁴ Longer half-lives allow for excretion studies to be performed and monitored over multiple days, rather than hours. This also aids in the localization of the annihilation events because the slower this process occurs the greater the likelihood of

pinpointing the appropriate site. With the field of immuno-PET ever expanding, the need for improved imaging agents has never been greater.

CHAPTER 1

COMPUTATIONAL ANALYSIS OF AND SYNTHETIC PROGRESS TOWARDS BIFUNCTIONAL NITROGEN BASED MACROCYCLES FOR IMMUNO-PET

Summary

In this chapter, the author will review the use of N-based macrocycles for metal ion coordination. The literature discussed pertains to 1,4,7-triazacyclononane (TACN) derivatives for hexadentate coordination of M^{3+} cations with a focus on Sc^{3+} . The author will also give a brief overview of the use of ^{44}Sc as a radiotracer for immuno-PET. Additionally, the computational analysis of Zr^{4+} tetraazamacrocycle derivatives and subsequent synthetic progress towards a novel bifunctional Sc^{3+} triazamacrocycle is discussed and outlined in Scheme 1-1.

Ligand Design for Sc-Based Radiotherapeutics

Over recent years, the octadentate chelator 1,4,7,10-tetraazacyclododecane-1,4,7,10-tetraacetic acid (DOTA) has entered the forefront for Sc^{3+} coordination due to its strong binding capabilities.²³ Difficulty arises with this chelator because the complexation kinetics are such that heating to upwards of 70 °C is required. This makes the conjugation of antibodies rather difficult because heating to such temperatures for extended periods of time can negatively affect these biomolecules. The ideal goal is to find a chelator with kinetically fast coordination at room temperature that is both stable and inert. Hexadentate chelators, such as 1,4,7-triazacyclononane-1,4,7-triacetic acid (NOTA), tend to coordinate Sc^{3+} faster, but are less inert which can lead to decomplexation of the metal center.²⁴

N-Based Macrocycles and Derivatives

Our research will be focusing on nitrogen-based macrocycles. An extensive amount of work has been performed on nitrogen-based linear chelators, most of which has proven incredibly useful. Using the flexibility of nitrogen's chelation properties as a Lewis base, many ligands have been successfully designed and have been used in post-clinical studies, as well active use in the medical field. Nitrogen-based macrocycles have been prevalent in coordination chemistry for many years, due to their intermediate polarizability as a Lewis base. N-based macrocycles can be used in a wide variety of coordination complexes, allowing TACN to coordinate transition metals across the periodic table from soft Cd^{2+} to hard Sc^{3+} .²⁵⁻²⁸ As stated, the macrocycle effect comes into play with these systems and is the increased affinity for metal cations of a macrocyclic system when compared to their linear analogues.²⁹

The first synthesis of TACN was reported by Koyama and Yoshino in 1972. This was done via the hydrolysis of its predecessor, 1,4-di-p-toluenesulfonyl-1,4,7-triazacyclononane, using hydrobromic acid and glacial acetic acid. The synthesis of 1,4-di-p-toluenesulfonyl-1,4,7-triazacyclononane was low yielding and therefore inefficient.³⁰ Later, Richman and Atkins reported a method employing sulfonamide leaving groups that can produce 9- to 21-membered macrocycles with differing amounts of heteroatoms. This method, followed by an oxidative cleavage of the tosyl groups and basification to the free amine provided large scale synthesis of a desired macrocycle.³¹

Computational Design of Phosphinate Containing N-Based Macrocyclic

The design for the triazamacrocyclic complex (**17**), seen in Figure 1-1 was derived from our computational work done on a tetraazamacrocyclic, phosphinate containing ligand for ^{89}Zr .

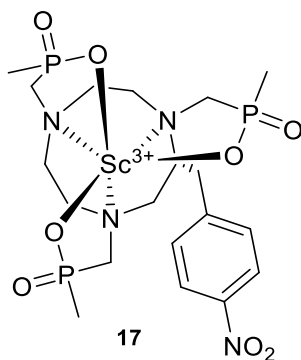


Figure 1-1: Structure of bifunctional triazamacrocyclic complex (**17**)

Chelators similar in design were employed by Wadas *et al.* in 2017 using cyclen as the backbone.³² The Zr chelators, Figure 1-1, were DOTA, DOTP, and DOTAM.

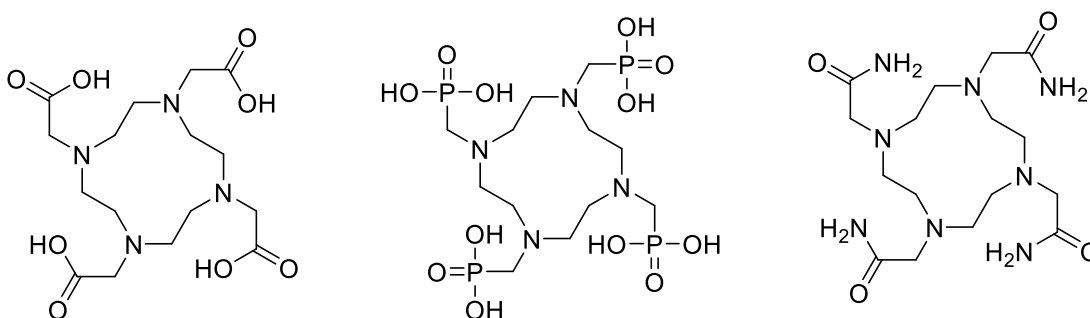


Figure 1-2: Structures of DOTA (left), DOTP (middle), and DOTAM (right)

This work showed significantly increased *in vivo* and *in vitro* complex stability when compared to Zr(DFO), the long-time gold standard for zirconium-based radiotherapeutics. While Zr(DOTA) showed the greatest complex stability, many groups have already focused on increasing this chelator's well-known potential and ⁸⁹Zr chelators in general.³³⁻⁴⁷ Our group was more interested in the phosphorus containing chelator DOTP. This structure employs phosphonate pendant groups in comparison to DOTA which contains carboxylic acid pendant groups. Wadas and coworkers found that due to the phosphonate containing pendant groups there

was an increase in retention of the radiolabeled complex in kidneys, liver, and bone tissue. This was attributed to numerous possibilities: transchelation to serum proteins, instability to lower pH cellular environments, or possible adsorption to bone matrices. The latter observation had been seen in other radiolabeled DOTP complexes and was mitigated by reducing the amount of phosphonate containing pendant arms in copper tetraazamacrocycles.⁴⁸

It was decided that further derivations of the DOTP chelator may lead to very insightful and intriguing outcomes, because extensive derivations to the DOTA chelator have already been performed. To aid in the synthetic design of such chelators, computational chemistry was performed. Our approach was to modify the phosphonate pendant arm to help minimize the chances of retention of the radiolabeled complexes. We hypothesized that the non-coordinating hydroxyl of the phosphonate group was a potential cause of this, because many interactions can occur. The most simplistic way of adjusting this structure was by changing the hydroxyl into a methyl group, a significantly less reactive moiety. The structure of DOTPi, derived from DOTP, can be seen above in Figure 1-2. A triaza analogue of DOTPi has been synthesized by Sherry and coworkers and was utilized for monitoring free Mg^{2+} by NMR spectroscopy.⁴⁹ Our synthetic work will focus on the functionalization of a triaza analogue of DOTPi and subsequent chelation with ^{44}Sc .

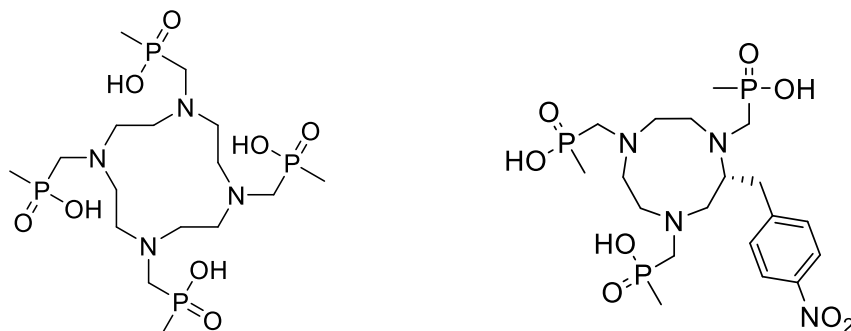


Figure 1-3: Structure of derived DOTPi and functionalized NOTPi

A tetraaza chelator would completely fill zirconium's desired coordination number of eight, with four oxygen groups donating and four nitrogen groups donating, and structures can be seen below in Figure 1-3. It has been hypothesized that the coordination of the hydroxyl groups of DOTP and DOTPi to the Zr^{4+} may be stronger than that of DOTA. This could be due to the increased electronegativity difference between O/P (EN difference ≈ 1.4) compared to O/C (EN difference ≈ 1.0). This increased difference in electronegativity could allow oxygen to have stronger binding to the electropositive metal ions. Coupling this with the derivation of the phosphonate group to methyl-phosphinate, could yield a complex with stronger binding properties.

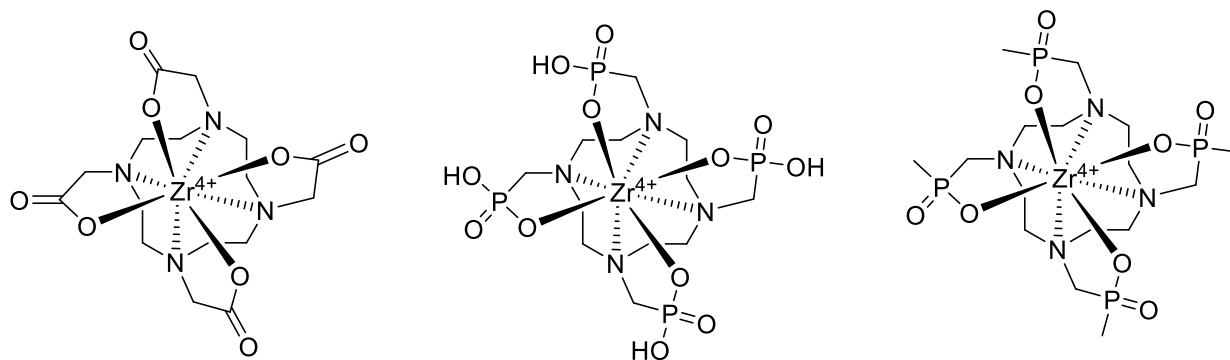


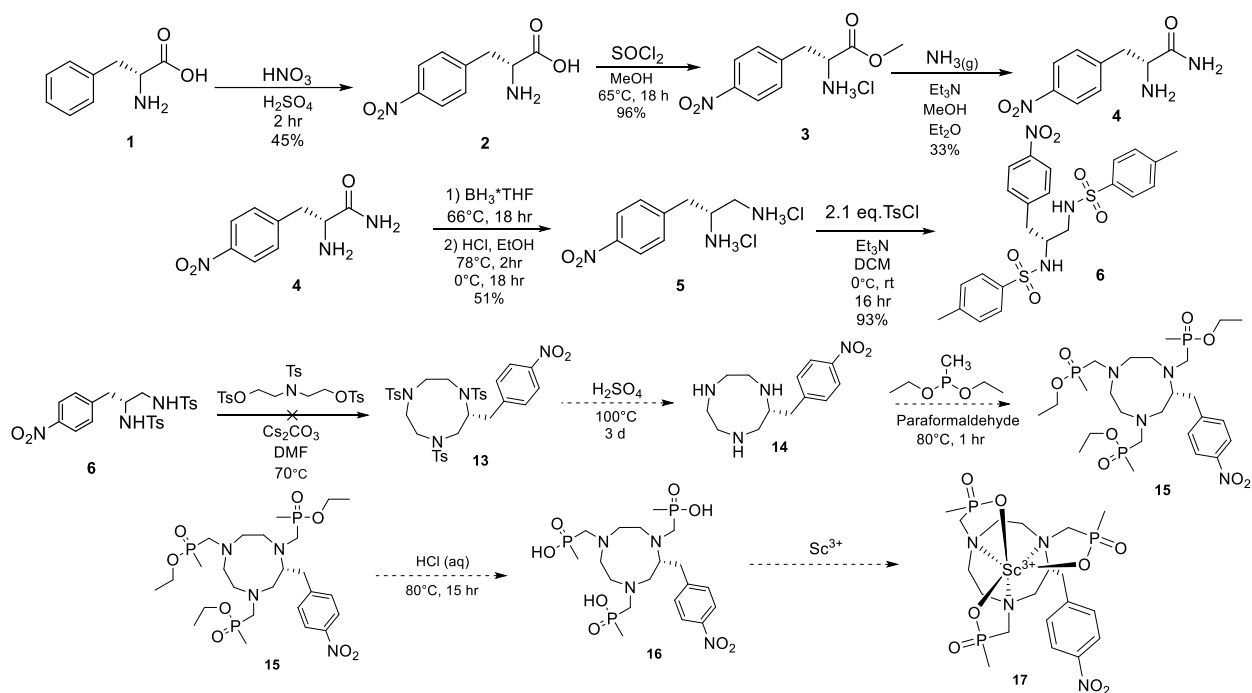
Figure 1-4: Structures of Zr^{4+} (DOTA) [left], Zr^{4+} (DOTP) [middle], and Zr^{4+} (DOTPi) [right].

For insight to the ligating ability of DOTPi, geometry optimizations were performed and compared for Zr^{4+} (DOTA), Zr^{4+} (DOTP), and Zr^{4+} (DOTPi). These calculations were performed using Gaussian '09 software at the DFT level. This study was mainly performed to analyze the coordinate covalent bond distances and chelate angles between the Zr^{4+} and ligand in each of the three complexes. These were then compared to bond lengths and angles of similar structures that had been accepted into the Cambridge Crystallographic Database Center.

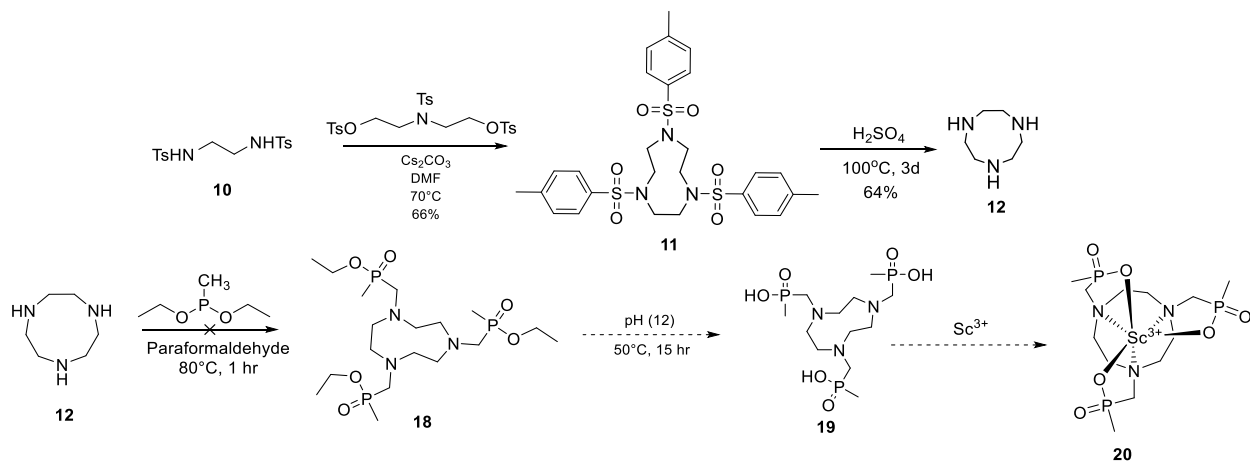
Zr⁴⁺(DOTA) was analyzed with a dual basis set of 6-31g* for the elements C, H, O, and N while the Zr⁴⁺ required a LANL2DZ pseudopotential. The other complexes Zr⁴⁺(DOTP) and Zr⁴⁺(DOTPi) required a triple basis set of: B3LYP 6-31g* for the elements C, H, O, and N, LANL2DZ pseudopotential for Zr⁴⁺, and a more diffuse basis set of B3LYP 6-311g** for P.

Work has also been performed that shows macrocyclic chelates, such as DOTA, can allow for water to enter the metal centers inner coordination sphere. This was shown when a chemistry group in the UK provided a crystal structure of [Y(DOTA)(H₂O)]⁻ and NMR evidence of [Zr(DOTA)(H₂O)].⁵⁰ These complexes allow for water to enter the 7th coordination site and 9th coordination site for Y and Zr respectively. The idea that water can enter the coordination sphere could lead to added instability within these complexes because it changes the desired coordination number.

This work, in combination with computational work done by undergraduate Johanna Pastoriza on a triazamacrocyclic analogue of DOTPi for Sc³⁺, led to the synthetic design of our final, bifunctional complex (**17**). Scheme 1-1 incorporates a bifunctional handle into the backbone of the macrocyclic system which can later be modified for conjugation to antibodies.⁵¹ A model system of (**17**), seen in Scheme 1-2, as (**20**) is the same scandium complex without the bifunctionality incorporated.



Scheme 1-1: Synthetic design of bifunctional complex (**17**) Sc^{III}(p-NO₂-Bn-NOTPi)



Scheme 1-2: Synthetic design of model complex (**20**) Sc^{III}(NOTPi)

Computational Results

Geometry optimizations of Zr⁴⁺(DOTA), Zr⁴⁺(DOTP), and Zr⁴⁺(DOTPi) were all completed using Gaussian '09 software. This was to analyze theoretical bond lengths to

understand if synthesis was worth pursuing. Figure 1-5 outlines results obtained from these calculations.

Key Bonds	Zr(DOTA)	Zr(DOTP)	Zr(DOTPi)
Zr-N	2.567 Å	2.597 Å	2.623 Å
Zr-O	2.104 Å	2.096 Å	2.093 Å
P-CH ₃	N/A	N/A	1.816 Å
P-OH	N/A	1.613 Å	N/A
C-O	1.317 Å	N/A	N/A

Figure 1-5: Key bond lengths calculated for Zr⁴⁺(DOTA), Zr⁴⁺(DOTP), and Zr⁴⁺(DOTPi)

While there wasn't as drastic a difference in the Zr-O bond length, we did see that bond length shorten from 2.104 Å in Zr(DOTA) to 2.093 Å in Zr(DOTPi). Even though this is only a decrease of ~.01 Å, this follows the trend we hypothesized based on the electronegativities of the atoms adjacent to the coordinating oxygen. The electronegativity difference between O/P (EN difference \approx 1.4) compared to O/C (EN difference \approx 1.0), this causes the bond to be more ionic in character leading to oxygen being a better Lewis base for zirconium.

Conversely, the Zr-N bond length increases from 2.567 Å in Zr(DOTA) to 2.623 in Zr(DOTPi). While this is only an increase of 0.056 Å, the difference is greater than that of the decrease in Zr-O bond length. This increase in bond length most likely comes from the greater steric hinderance due to the increased bulkiness of the substituents in DOTPi vs DOTA. Another attribution could be due to the rigidity of these tetraazamacrocycles. This rigidity may not allow the macrocycle to be able to compensate for the decrease in Zr-O bond length. Furthermore,

nitrogen isn't considered a hard Lewis base, and there isn't a powerful enough drive to prevent the slight increase in bond length.

Because that these complexes allow for the addition of water into the 9th coordination site of zirconium⁵⁰, calculations were performed on $[\text{Zr}^{4+}(\text{DOTA})(\text{H}_2\text{O})]$, $[\text{Zr}^{4+}(\text{DOTP})(\text{H}_2\text{O})]$, and $[\text{Zr}^{4+}(\text{DOTPi})(\text{H}_2\text{O})]$. These complexes, seen below in Figure 1-3, could potentially help explain the *in vivo* instability.

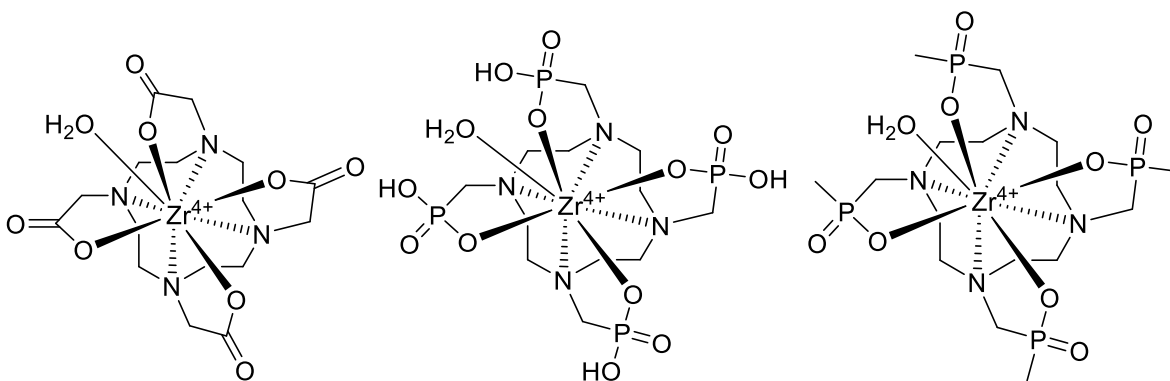


Figure 1-6: Structures of $[\text{Zr}^{4+}(\text{DOTA})(\text{H}_2\text{O})]$ {left}, $[\text{Zr}^{4+}(\text{DOTP})(\text{H}_2\text{O})]$ {middle}, and $[\text{Zr}^{4+}(\text{DOTPi})(\text{H}_2\text{O})]$ {left}

These structures are the same as the ones previously discussed, except for each having an additional water included into the zirconium's 9th coordination site. To analyze the effects of this addition of water, similar computations were performed on their non-water analogues and their results are summarized in Figure 1-7 below.

Key Bonds	[Zr(DOTA)(H₂O)]	[Zr(DOTP)(H₂O)]	[Zr(DOTPi)(H₂O)]
Zr-N	2.647 Å	2.689 Å	2.714 Å
Zr-O	2.137 Å	2.111 Å	2.115 Å
P-CH ₃	N/A	N/A	1.818 Å
P-OH	N/A	1.619 Å	N/A
C-O	1.317 Å	N/A	N/A
Zr-OH ₂	2.397 Å	2.540 Å	2.519 Å

Figure 1-7: Key bond lengths calculated for [Zr⁴⁺(DOTA)(H₂O)], [Zr⁴⁺(DOTP)(H₂O)], and [Zr⁴⁺(DOTPi)(H₂O)]

It is immediately noticeable that the Zr-N bond length in every case is longer than that of the longest Zr-N bond without any water coordinated. This is especially true for the [Zr⁴⁺(DOTPi)(H₂O)] complex as the Zr-N bond length becomes over 2.7 Å. This is now leaving the range of known crystal structures with similar types Zr-N bonds. Bonds of this length are generally considered unstable because the coordination strength becomes weaker as the bond length increases. It is of note that the Zr-O bond lengths do not have a drastic increase in length, but a similar trend is seen where the phosphorus containing structures have shorter Zr-O bond lengths.

Synthesis of Bifunctional Sc³⁺ Chelator for Immuno-PET

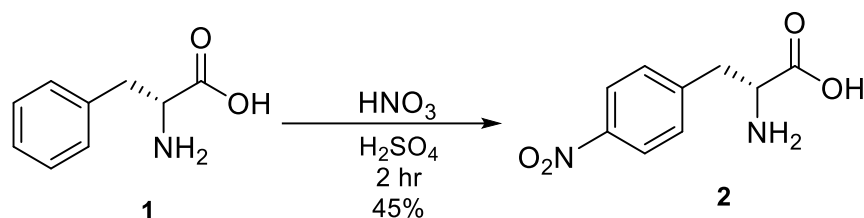


Figure 1-8: Nitration of L-Phenylalanine

L-phenylalanine (**1**) was first subjected to an electrophilic aromatic substitution using a mixture of concentrated nitric acid and catalytic sulfuric acid to implement bifunctionality into the backbone of the chelator. This yielded 4-nitro-L-phenylalanine (**2**) in 45% yield following purification via recrystallization from deionized water. This was evidenced by the characteristic splitting pattern of para-substituted aromatic rings and can be seen in Figure 1-9 and appears all of the following ¹H NMR.

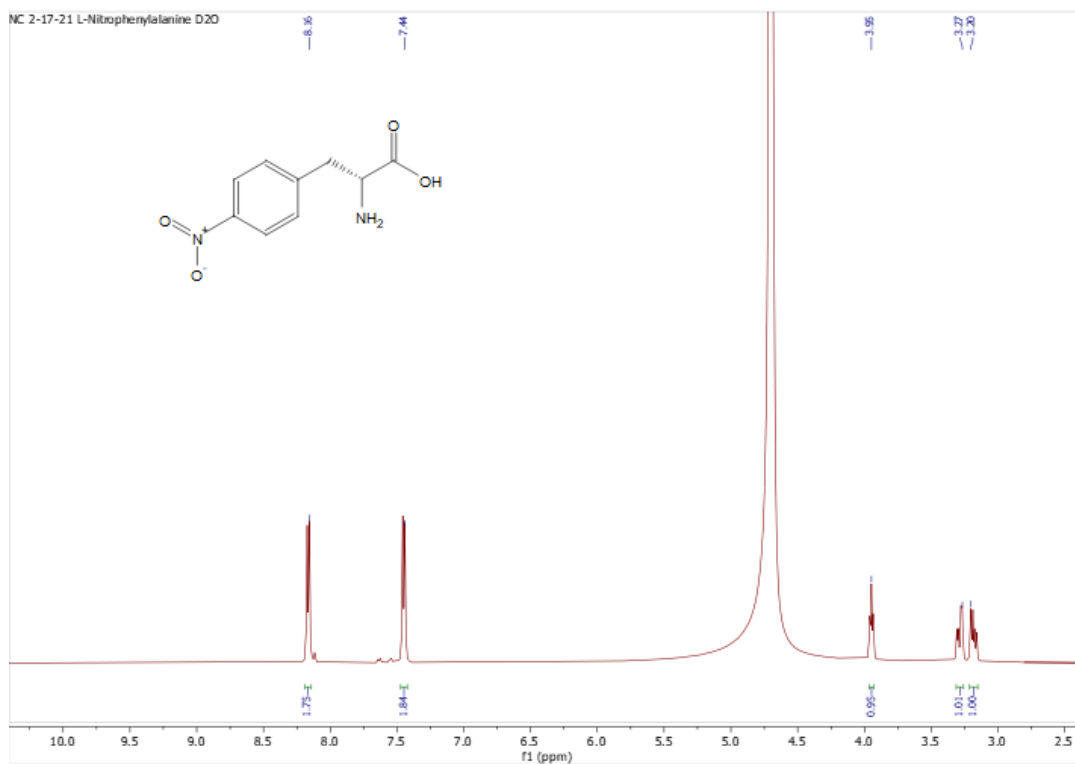


Figure 1-9: ¹H NMR of 4-nitro-phenylalanine

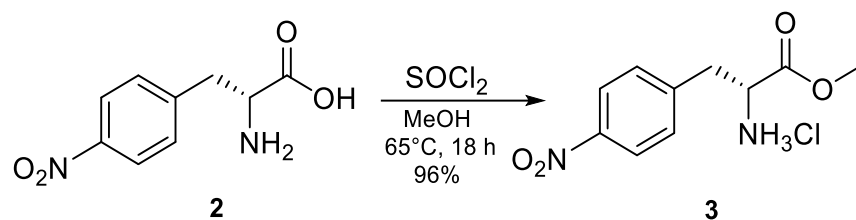


Figure 1-10: Formation of methyl ester via SOCl_2

4-nitro-L-phenylalanine (**2**) was then converted to the methyl ester hydrochloride salt (**3**) via the *in-situ* formation of the acyl chloride with thionyl chloride in methanol. This method was utilized due to the fast reaction time and minimal workup, including only the evaporation of solvent. Analytically pure (**3**) was characterized via the appearance of a methyl peak on ^1H NMR.

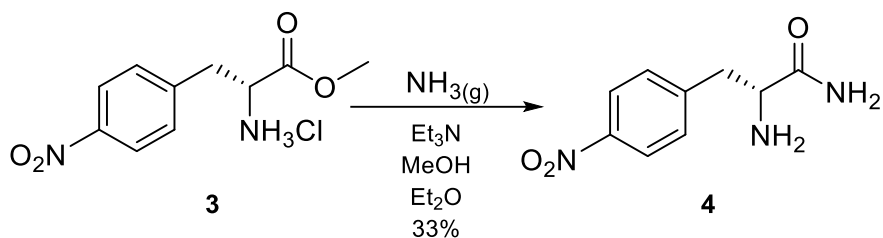


Figure 1-11: Formation of amide

The methyl ester (**3**) was converted to the amide (**4**) following the neutralization of the hydrochloride salt with Et_3N in Et_2O , removal of triethylammonium chloride and concentration of the filtrate. This amino ester was dissolved in dry MeOH, saturated with $\text{NH}_3(\text{g})$, and allowed to sit at -15°C until conversion to (**4**) was complete. Although yields were low, pure material was collected via removal of excess $\text{NH}_3(\text{g})$ and subsequent evaporation of solvent. Conversion of (**3**) to (**4**) was confirmed via the formation amide NH_2 protons seen in ^1H NMR

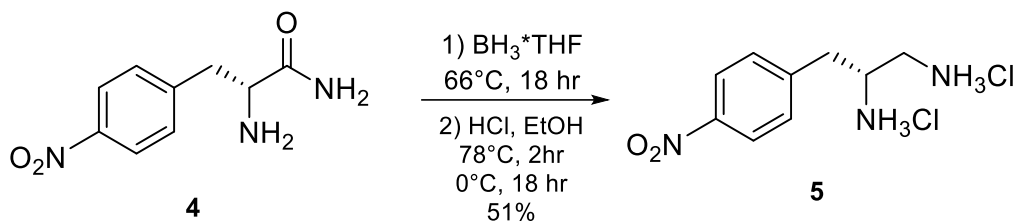


Figure 1-12: Formation of diamine dihydrochloride salt

The reduction of the primary amide (4) was completed using 1 M BH₃*THF complex in dry, distilled THF under inert atmosphere. After quenching with MeOH, residue is taken up into absolute EtOH and saturated with HCl(g) to yield the dihydrochloride diamine (5). This product was confirmed with the disappearance of the amide carbon using ¹³C NMR and the appearance of a second set of diastereotopic protons in ¹H NMR because of the resulting methylene formation.

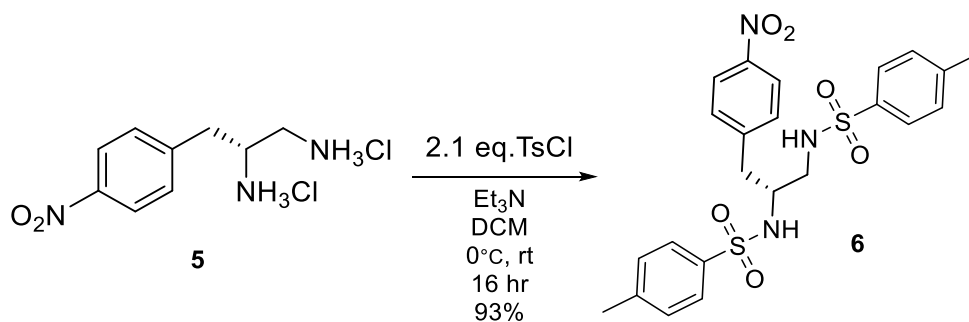


Figure 1-13: Formation of ditosyl diamine

Conversion of (5) to (6) was performed via the neutralization of the diamine and subsequent addition of recrystallized tosyl chloride. The result product was purified from dry MeOH leading to analytically pure (6). This can be evidenced from the appearance of inequivalent methyl protons from each tosyl group and can be seen in ¹H NMR. It is interesting to note that compound (6) has the potential to react with many different O-tosylate molecules to

increase or decrease the size of the macrocycle desired. In this work, the author focused on synthesizing the triaza macrocycle using tritosyl diethanolamine.

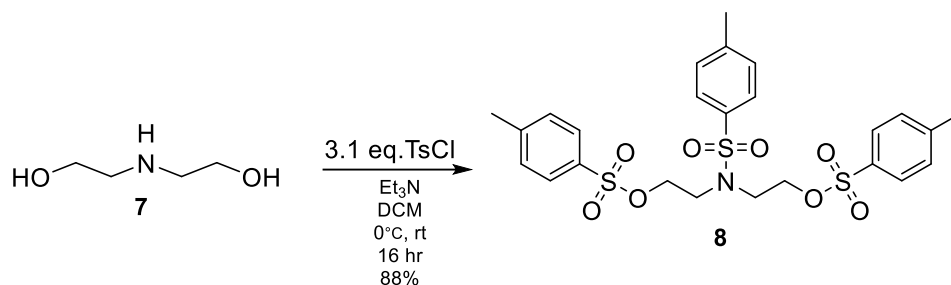


Figure 1-14: Formation of tritosyl diethanolamine

To form the desired triazamacrocycle, the synthesis of the tritosyl diethanolamine (**8**) was required. This was performed via the addition of recrystallized tosyl chloride to a solution diethanolamine. After purification via recrystallization from ethanol, analytically pure (**8**) was produced. This symmetric molecule has a C₂ axis of rotation about the nitrogen leading to many equivalent protons via NMR. The appearance of four aromatic doublets and two aliphatic singlets can appropriately identify this molecule and the ¹H NMR.

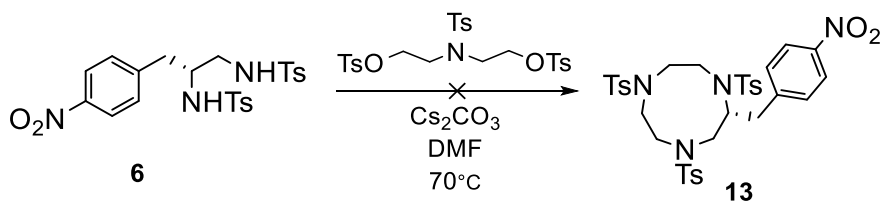


Figure 1-15: Attempted cyclization to p-NO₂-Bn-Tritosyl TACN

Attempts to perform a modified Richman-Atkins style cyclization of (**6**) to (**13**) have thus far been unsuccessful. By exposing the ditosyl diamine to a base such as Cs₂CO₃ the aim was to deprotonate the sulfonamides. This could then perform a nucleophilic attack to displace the tosyl

leaving groups, resulting in the desired cyclization. No definitive results have been acquired. Potential to incorporate the bifunctional nitro group after cyclization could lead to promising results, as the deactivating nature of the nitro group could diminish the nucleophilicity of the protected amines.

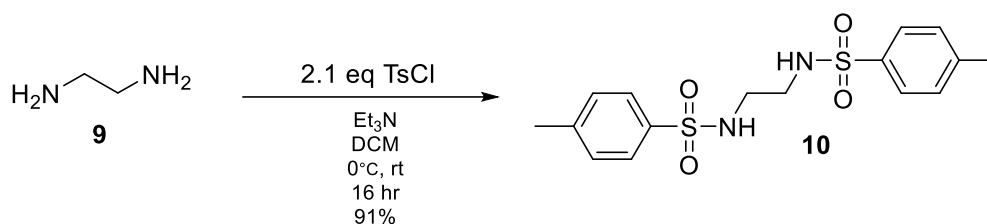


Figure 1-16: Formation of ditosyl ethylenediamine

To synthesize a model substrate of our final chelator, (**10**) was made and is analogous to (**6**) but does not incorporate the same bifunctionality. Ethylenediamine (**9**) was subjected to tosyl chloride in DCM. The resulting solid has a C₂ axis about the bond between the methylene carbons and results in many peaks being similar via NMR. The product was evidenced via the appearance of an aliphatic methyl peak and can be seen in the ¹H NMR.

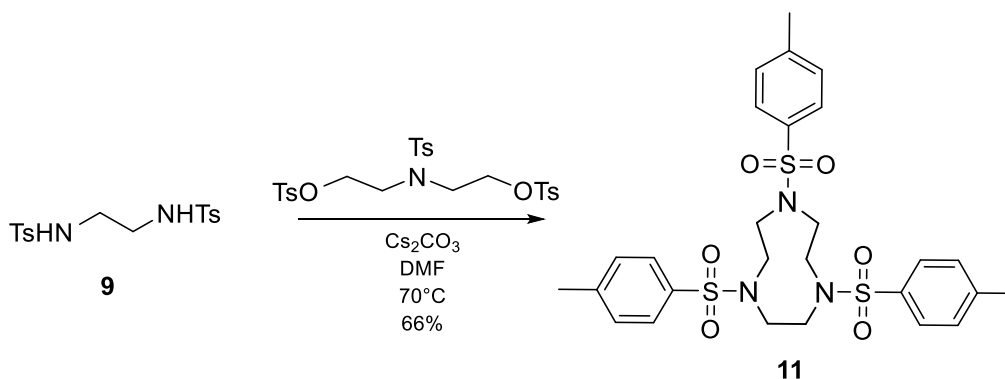


Figure 1-17: Richman-Atkins cyclization to tritosyl TACN

The Richman-Atkins cyclization to form (**11**) was successfully performed as for the attempted preparation of (**13**). Two conditions for this cyclization were attempted, in which LiH or Cs₂CO₃ was the base. Both were successful, but the latter was chosen due to the ease of workup by the precipitating product via addition of cold water to the reaction flask. This molecule has a C₃ axis about the center of the macrocycle and leads all three tosyl groups, and methylene protons, to be equivalent via ¹H NMR.

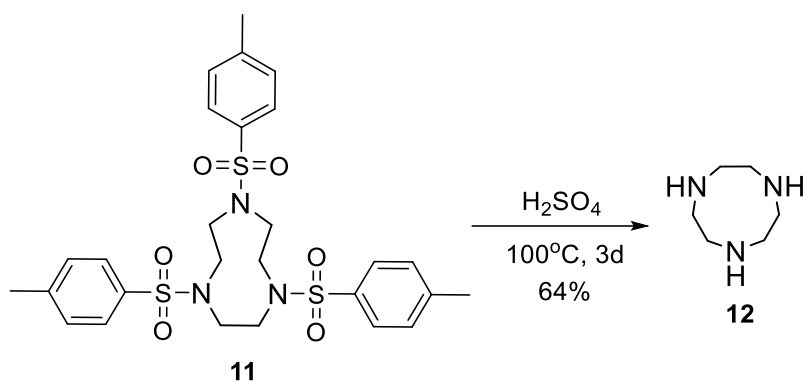


Figure 1-18: Formation of TACN

With the tosyl amides being a very strong protecting group, rigorous conditions were required to remove them. The deprotection to TACN (**12**) needed several days in hot concentrated sulfuric acid to properly remove the tosyl groups. Furthermore, to isolate the free base of TACN also required specific purification procedures. TACN had a strong tendency to hold onto the organic layer of DCM and so it was dried on a Schlenk line overnight to result in an analytically pure substance. The deprotection was evidenced via the disappearance of any aromatic protons of the sulfonyl groups and the appearance of the amine protons can be seen in ¹H NMR.

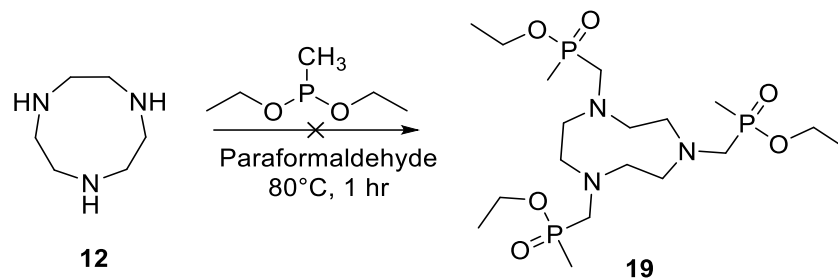


Figure 1-19: Attempted formation of phosphinate derivative of TACN

Thus far one attempt has been made to add phosphinate functionality onto an unprotected macrocyclic system and the synthesis of (**19**) has been unsuccessful. The proposed reaction would proceed via a phospho-Mannich style mechanism. The inclusion of a phosphinate moiety reduces the number of pendant oxygens which could perform unwanted chemistry *in vivo*. Literature precedent has shown this reaction to work and a subsequent hydrolysis of the methyl ethyl phosphinate results in a hexadentate chelator.⁴⁸

Conclusions and Future Work

Progress towards the synthesis of our final, bifunctional chelator (**17**) has been completed to the ditosyl diamine (**6**). This molecule has the potential for Richman-Atkin's cyclization and the production of a bifunctional N-based macrocycle with pendant phosphinate groups. This ligand is intended for Sc³⁺ based PET and may prevent dissociation from the metal, avoiding unwanted toxic metals being deposited throughout the body. Modelling this cyclization via the synthesis of TACN (**12**) has been successful and proves the viability of this method for the synthesis of the final chelator.

Future work includes completing the model ligand and bifunctional macrocycle synthesis, including methyl phosphinate pendant arms. Subsequent complexation studies with

Sc³⁺ could then be performed to analyze strength of coordination. The completion of the model ligand would allow for proof of concept for phosphinate pendant groups' to coordinate potential M³⁺ cations. Due to the difficulty in synthesis, phosphinate ligand are not extremely well studied and looking into their binding properties could open a wide variety of potential phosphinate moieties to be used in metal complexation.

CHAPTER 2

DESIGN AND SYNTHETIC PROGRESS TOWARDS A NOVEL BIFUNCTIONAL CHELATOR FOR ^{89}Zr AND IMMUNO-PET

Summary

In this brief chapter, the author will present the use of ^{89}Zr as a radiotracer for immuno-PET. Here, the candidate will also discuss the mechanism by which these bifunctional chelators can be selectively attached to antibodies. Additionally, the design and synthetic progress towards a high-affinity bifunctional chelator, for Zr^{4+} , derived from well-known siderophore deferoxamine B (DFO) will also be discussed and is outlined in Scheme 2-1.

Ligand Design for Zr-Based Radiotherapeutics

Chelating of ^{89}Zr has been studied by many families of chelators including: diethylenetriaminepentaacetic acid (DTPA), ethylenediaminetetraacetic acid (EDTA), 1,4,7,10-tetraazacyclododecane-1,4,7,10-tetraacetic acid (DOTA), and deferoxamine (DFO) with mixed results. DOTA, and its derivatives, have been addressed computationally in comparison to TACN in Chapter 1. This chapter will focus on the use of DFO and potential derivatives for Zr^{4+} chelation and further conjugation to antibodies.

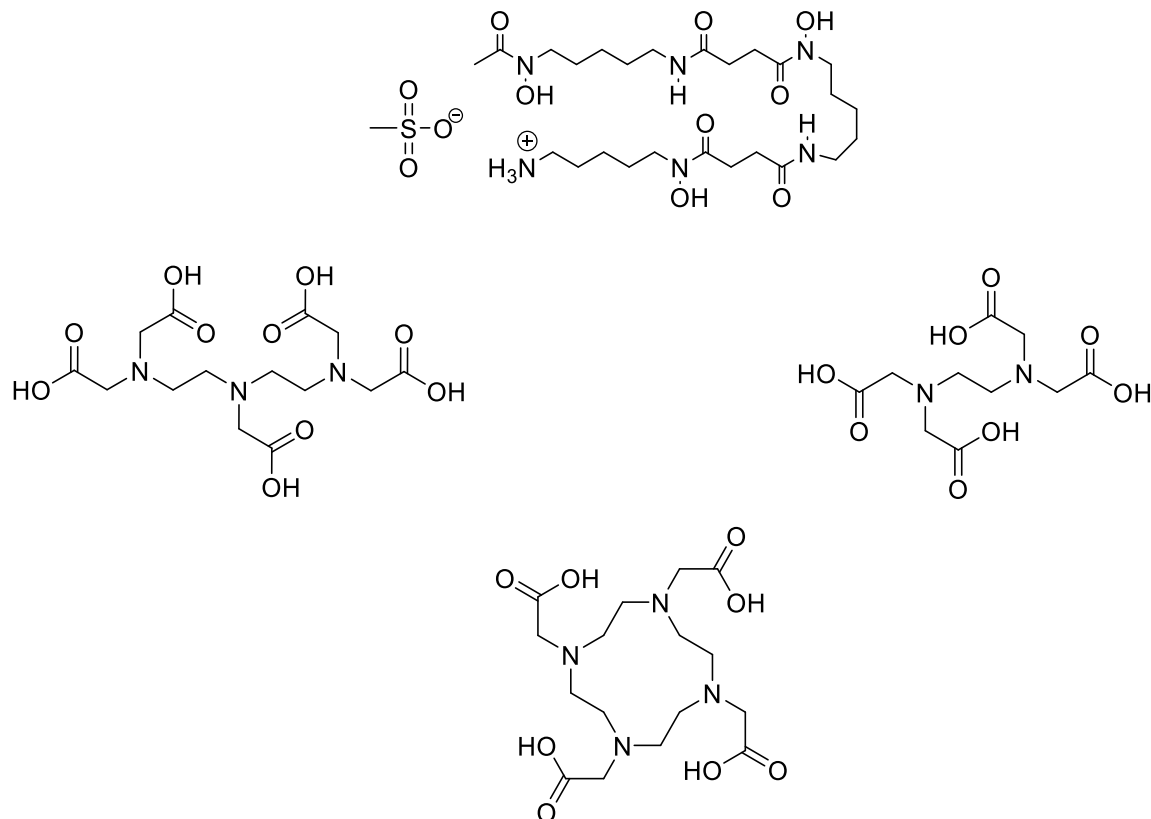
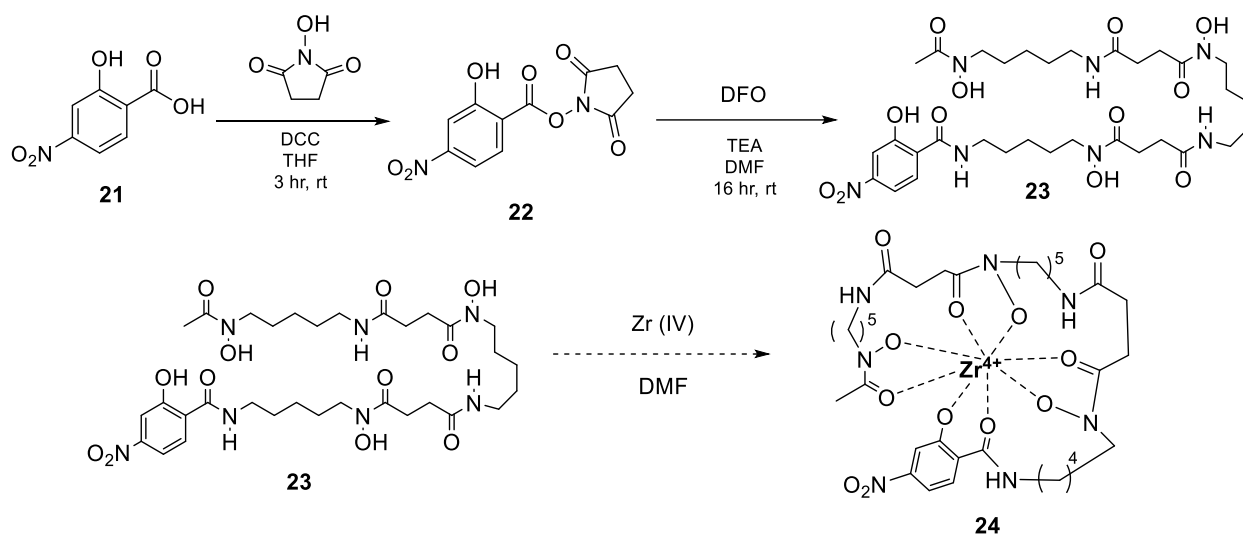


Figure 2-1: Structures of DFO (top), DTPA (left), EDTA (right), and DOTA (bottom).

Deferoxamine B (DFO)

DFO, seen above in Figure 2-1, is a hexadentate siderophore comprised of three hydroxamate moieties. Hydroxamate is a hard base chelating group theoretically ideal for the hard acid, Zr^{IV}. Classically known as an Fe³⁺ chelator, DFO has been of significant interest in Zr⁴⁺ coordination for its potential for immunoPET.⁵² The terminal primary amine of DFO is a perfect candidate for derivation to an octadentate system or direct conjugation to antibodies.^{53,54} Scheme 2-1, seen below, shows the synthetic route towards our final bifunctional complex Zr^{IV}(p-NO₂-Sal-DFO) (**24**).



Scheme 2-1: Synthesis of bifunctional complex (**24**) $Zr^{IV}(p\text{-NO}_2\text{-Sal-DFO})$

Synthesis of Bifunctional Zr^{4+} Chelator

To create a bifunctional, octadentate chelator we sought to functionalize the N-terminus of deferoxamine (DFO) with a p-NO₂-salicylic acid moiety. By increasing the denticity in such a way, the inclusion of two more hard acid donors became available to encapsulate the coordination sphere of zirconium. While not a hydroxamate group, the salicylic acid has a similar coordination method with the donors being a hydroxyl group and an amide carbonyl.

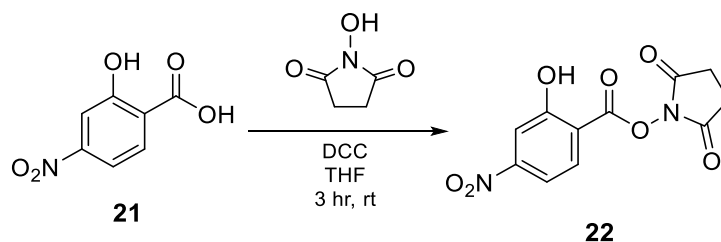


Figure 2-2: Synthesis of active ester

4-nitrosalicylic acid (**21**) was purchased and subjected to a DCC (N,N'-dicyclohexylcarbodiimide) coupling reaction with N-hydroxysuccinimide to afford the active

ester (**22**). This reaction was done with 4Å molecular sieves in the reaction flask to sequester the water byproduct and drive reaction towards products. This active ester would readily amidate DFO at the terminal position. The ¹H NMR of **22** identifies product formation via the appearance of symmetric methylene protons.

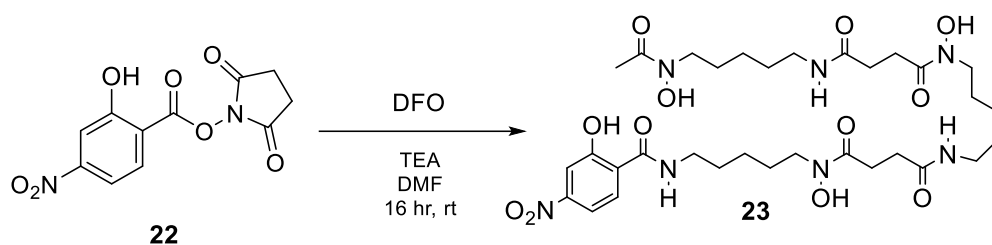


Figure 2-3: Functionalization of DFO-NH₂

The synthesis of (**23**) was proven to be successful via a TOF ESI-MS and can be seen in Figure 2-5 and calculated for C₃₂H₅₂O₁₂N₇: 726.3596; found: 726.3677. NMR spectra were difficult to obtain because separation of unreacted DFO from (**23**) was challenging. The similar chemical environment between the two resulted in DFO that was not consumed which can be seen at *M/Z* of 561.3607. Since there was unconsumed DFO, complexation with ⁸⁹Zr would result in a product mixture unsuitable for analysis or radiotherapeutic use. Thus, complexation reactions are not yet viable.

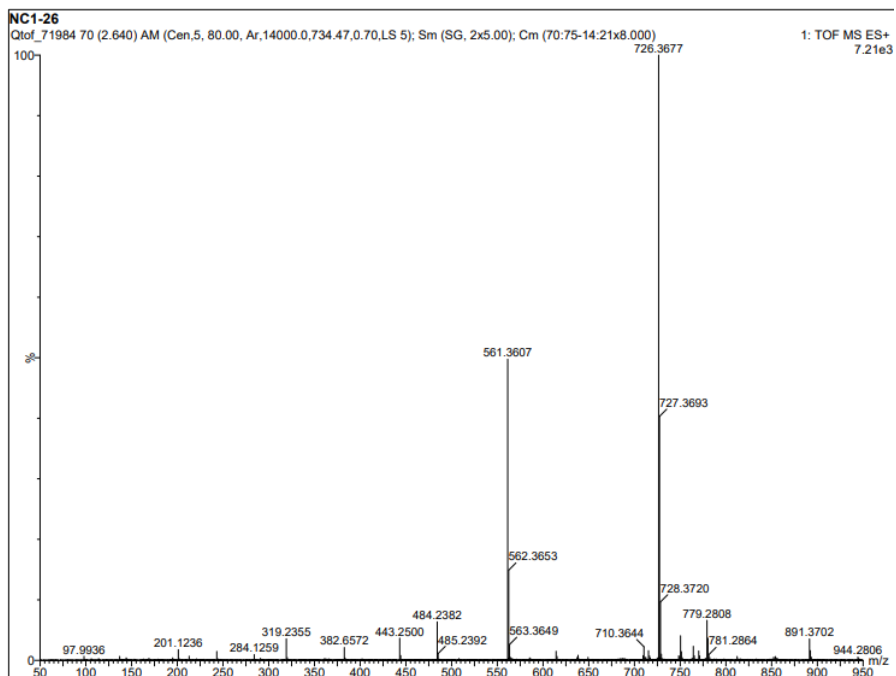


Figure 2-4: TOF ESI-MS of functionalized DFO

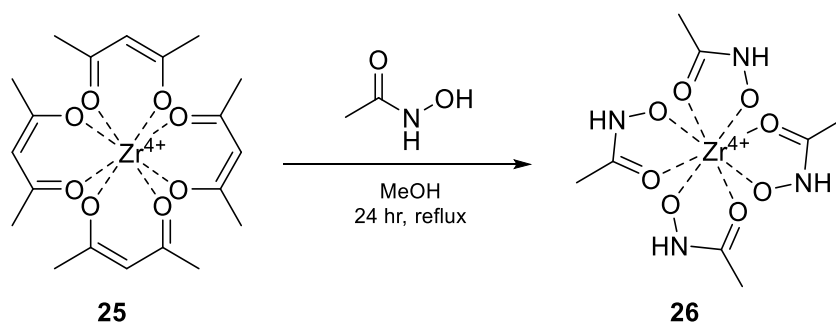


Figure 2-5: Synthesis of $\text{Zr}^{\text{IV}}(\text{AHA})$

To assess the coordination ability of the hydroxamate group as a donor, $\text{Zr}^{\text{IV}}(\text{acac})$ was reacted with aceto-hydroxamic acid as a model for DFO. Shortly after reflux began, a white precipitate formed. ^{13}C NMR spectrum of **26** shows product formation as there is one peak for the methyl and hydroxamic acid carbon while the starting material would show three carbon peaks.

Conclusions and Future Work

Using TOF ESI-MS, it was confirmed that the p-NO₂-salicylic acid derivative of DFO (**23**) was synthesized. Unfortunately, the separation of unconsumed DFO from desired product is still a challenge. This project was suspended with the possibility of using preparative or a flash chromatography method to purify **23**. If **23** were pure, the reaction with Zr^{IV}(acac) according to Figure 2-6 could be viable. The novel chelator **23** could lead to exciting insights into the coordination strength of Zr(DFO) complexes and subsequent improvements of *in vivo* zirconium based radiotherapeutics.

CHAPTER 3

Experimental Section

General Methods

Solvents and Reagents

All solvents and reagents were purchased from Fisher, Alfa Aesar, Sigma Aldrich, Pharmco Aaper, and Acros. Most chemicals were used as-is and required no further purification. Tosyl chloride was purified via recrystallization from petroleum ether to remove any tosic acid.⁶⁵

Reactions

Reaction glassware and magnetic stir bars were stored in an oven at 200°C prior to use. Unless otherwise stated, all reactions were performed under inert atmosphere.

Spectroscopy

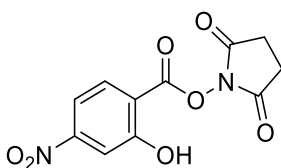
Nuclear Magnetic Resonance (NMR) spectroscopy characterized all intermediates and final products. ¹H NMR was acquired with a Varian Mercury 500 MHz NMR and ¹³C NMR with a Varian Mercury 125 MHz NMR. Chemical shifts are reported in parts per million (ppm) relative to tetramethylsilane (TMS) unless otherwise noted. CDCl₃, DMSO-d₆, and D₂O were all

purchased from Cambridge Isotope Labs. The following abbreviations were used to denote the corresponding multiplicities: s = singlet, d = doublet, t = triplet, q = quartet, p = pentent, dd = doublet of doublets, m = multiplet.

Quantum Chemical Calculations

The quantum chemical calculations were performed with complete geometry optimization without any symmetry restrictions. All analyses were performed with the Gaussian '09 software. Geometries of the studied compound were optimized using the DFT method and a hybrid B3LYP functional. The basis set used to optimize the ligand was 6-31G*(d,p) carbon, oxygen, nitrogen, and hydrogen. This was not sufficient for heavier elements and the LANL2DZ pseudopotential basis set was used in combination with simpler basis sets for the metal complexes. Any computation that included the element phosphorus required a more diffuse basis set, and the 6-311G**(d,p) was used allowing for more accurate depictions of the “tail” end of atomic orbitals including phosphorus, which is a larger, softer ion.

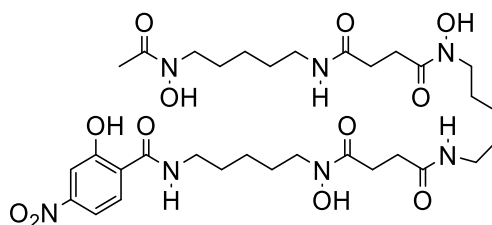
Detailed Experimental



2,5-Dioxo-1-pyrrolidinyl 2-hydroxy-4-nitrobenzoate (22)

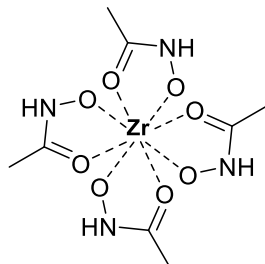
In a 100 ml round bottom flask, 2-hydroxy-4-nitrobenzoic acid (**21**) (1.17g, 6.40 mmol), N-hydroxysuccinimide (1.20g, 10.8 mmol), and N,N'-dicyclohexylcarbodiimide (1.30 g, 6.50 mmol) was dissolved in THF (25 mL) and was set to stir at 25°C under N₂ gas for 3 hours. Over 3 hours, a white precipitate was formed and filtered off via vacuum filtration. The filtrate was

concentrated under reduced pressure to yield a light brown solid. Following a recrystallization in DCM, pure (**22**) (622 mg, 45.0% yield) was collected as a light brown solid: ^1H NMR (500 MHz, CDCl_3) δ 8.13 (d, $J=8.85$ Hz, 1H), δ 7.82 (d, $J=2.28$ Hz 1H), δ 7.72 (dd, $J=6.57$ Hz, $J=2.13$ Hz, 1H), δ 2.89 (s, 4H). ^{13}C NMR (125 MHz, CDCl_3) δ 168.3, 164.2, 162.9, 153.3, 131.7, 114.3, 113.9, 113.0, 25.7.



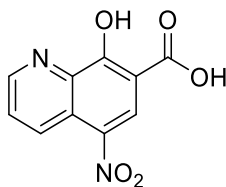
p-NO₂-Sal-DFO (**23**)

2,5-Dioxo-1-pyrrolidinyl 2-hydroxy-4-nitrobenzoate (**22**) (0.640 g, 2.28 mmol) was dissolved in DMF (25 mL) in a 100 mL round bottom flask. To this, deferoxamine mesylate (500 mg, 0.760 mmol) and triethylamine (117 μL , 0.800 mmol) were added and set to stir at 70°C for 20 hours under N₂. The precipitate was collected via vacuum filtration, and the product was washed with cold acetone and water to remove impurities, and (**23**) was collected as an orange solid. This solid was then lyophilized for two days to yield an orange/yellow powder. ESI-HRMS (m/z): $[\text{M} + \text{H}]^+$ calculated for C₃₂H₅₂O₁₂N₇: 726.3596; found: 726.3677.



Zr^{IV} (Acetohydroxamate) (26)

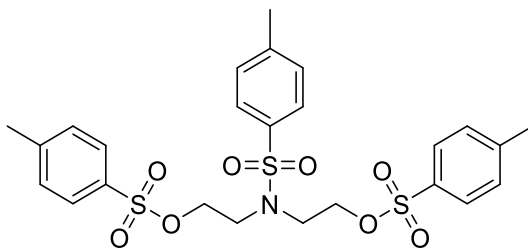
Zr^{IV} (Acetylacetonate) (525 mg, 1.08 mmol) was placed in a 250 mL round bottom flask and dissolved in dry methanol (40 mL). To this, a solution of acetohydroxamic acid (363 mg, 4.80 mmol) in dry methanol (50 mL) was added and set to reflux under N₂ for 24 hours. After cooling, a white precipitate was collected via vacuum filtration and rinsed with cold methanol. Zr^{IV} (Acetohydroxamate) (398 mg, 87.3% yield) was collected as a white solid. ¹H NMR: (500 MHz, D₂O) δ 1.92 (s, 12H).



5-NO₂-7-Carboxy-8-Hydroxyquinoline

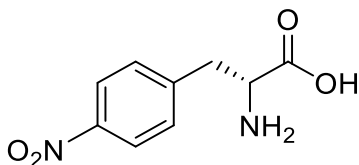
7-Carboxy-8-Hydroxyquinoline (945 mg, 5.00 mmol) was dissolved in concentrated H₂SO₄ (10 mL) and set to stir at 0°C. To this, concentrated HNO₃ (1 mL) was added dropwise and left to stir at 0°C for 25 minutes. This solution was then poured into an ice-cold purified water bath to precipitate a yellow solid, which was then collected via vacuum filtration. To remove any potential impurities, the product was further washed with ice-cold water and methanol. Pure 5-NO₂-7-Carboxy-8-Hydroxyquinoline (1.08 g, 92.3% yield) was collected as a

vibrant yellow solid. ^1H NMR (500 MHz, DMSO-d_6) δ 9.77 (dd, $J=7.47$ Hz, $J=1.37$ Hz 1H), δ 9.02 (dd, $J=3.66$ Hz, $J=1.38$ Hz, 1H), δ 8.98 (s, 1H), δ 8.25 (dd, $J=5.04$ Hz, $J=3.80$ Hz 1H).



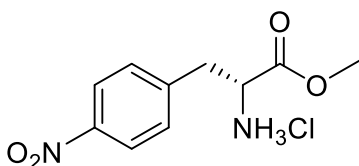
Tritosyl Diethanolamine (8)

Diethanolamine (**7**) (5.50g, 52.4 mmol) was placed in a 500 mL round bottom flask and dissolved in dry DCM (100 mL). This solution was cooled to 0°C , and Et_3N (24.4 mL, 176 mmol) was added under N_2 . While stirring at 0°C tosyl chloride (31.4g, 164 mmol), recrystallized from petroleum ether, in dry DCM (100 mL) was added dropwise over 1 hour. The reaction mixture was then set to stir at 25°C overnight. The pale-yellow solution was then washed with 2.5 M aqueous HCl (3 x 50 mL), followed by H_2O (5 x 50 mL), and finally saturated aqueous NaHCO_3 (5 x 50 mL). The organic layer was then dried with NaSO_4 , and the solvent was reduced via vacuum. Following recrystallization in EtOH, (**8**) (25.6g, 87.7% yield) was collected as a white solid. ^1H NMR: (500 MHz, CDCl_3) δ 7.74 (d, $J=8.24$ Hz, 4H), δ 7.59 (d, $J=8.24$ Hz, 2H), δ 7.34 (d, $J=*.26$ Hz, 4H), δ 7.26 (d, $J=8.24$ Hz, 2H), δ 4.11 (t, $J=5.95$ Hz, 4H), δ 3.36 (t, $J=6.10$ Hz, 4H), δ 2.44 (s, 6H), δ 2.40 (s, 3H). ^{13}C NMR: (125 MHz, CDCl_3) δ 145.3, 144.2, 132.4, 130.1, 130.0, 127.9, 127.2, 127.0, 68.3, 48.4, 21.7, 21.5.



p-NO₂-L-phenylalanine (**2**)

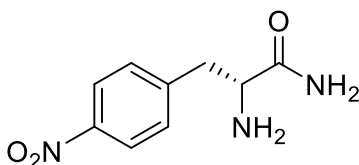
L-Phenylalanine (**1**) (30.01g, 181.7 mmol) was dissolved in concentrated H₂SO₄ (90 mL) before allowing to stir at 0°C. 40% HNO₃ (42.5 mL) that had previously been cooled to 0°C was added dropwise to this solution. This solution was then allowed to stir for a further 2 hours at 25°C. The solution was then poured into ice-cold purified water and neutralized using NaOH until pH was 4, allowing for a tan solid precipitation. The product was then isolated via vacuum filtration followed by washings with cold water. (**2**) (17.4g, 45.2% yield) was then recrystallized from deionized water as a tan crystal solid. ¹H NMR: (500 MHz, D₂O) δ 8.16 (d, J=8.54 Hz, 2H), δ 7.45 (d, J=8.55 Hz, 2H) δ 3.97 (t, J=6.1 Hz 1H), δ 3.28 (dd, J=8.54 Hz, J=5.8 Hz, 1H) δ 3.23 (dd, J=8.54 Hz, J=5.8 Hz, 1H).



p-NO₂-L-phenylalanine methyl ester (**3**)

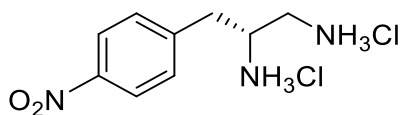
p-NO₂-L-phenylalanine (**2**) (18.0 g, 72.9 mmol) was placed into a 1 L round bottom flask along with dry methanol (400 mL) and set to stir at 0°C for 30 minutes under N₂. Thionyl chloride (6.90 mL, 95.1 mmol) that had been chilled to 0°C was added dropwise via glass syringe to this suspension. Once added, the solution was then allowed to reflux for 48 hours under constant N₂ flow to aid in removing SO₂ and HCl gases. The solvent was concentrated under reduced pressure to yield (**3**) (18.2 g, 95.6% yield) as a fluffy white solid without further

purification. ^1H NMR: (500 MHz, D_2O) δ 8.13 (d, $J=8.69$ Hz, 2H), δ 7.43 (d, $J=8.70$ Hz, 2H), δ 4.46 (t, $J=7.02$ Hz, 1H), δ 3.76 (s, 3H), δ 3.38 (dd, $J=7.94$ Hz, $J=6.56$ Hz, 1H), δ 3.30 (dd, $J=7.94$ Hz, $J=6.56$ Hz, 1H).



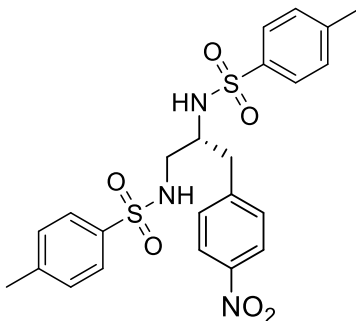
p-NO₂-L-phenylalanine amide (**4**)

p-NO₂-L-phenylalanine methyl ester (**3**) (20.1 g, 76.7 mmol) was placed into a 1 L round bottom flask with dry diethyl ether (390 mL), dry methanol (10 mL), and triethylamine (11.9 mL, 84.8 mmol) that had been dried with sieves. This suspension was set to stir at -78°C for 1 hour under N_2 atmosphere. The precipitated triethylamine hydrochloride salt was then filtered via cannula filtration. The pale-yellow filtrate was collected in a separate 1 L round bottom flask that had been previously purged with N_2 . The filtrate was then concentrated under reduced pressure to yield a dark yellow oil to which dry methanol (400 mL) was added and then set to cool to -15°C . Once cooled, $\text{NH}_3(\text{g})$ was bubbled in until the solution was saturated. The flask was then stoppered and placed into a -10°C freezer for 48 hours. Excess $\text{NH}_3(\text{g})$ was then carefully allowed to evaporate by warming flask in a warm water bath. The solvent was concentrated under reduced pressure to (**4**) (5.31 g, 32.7% yield) as an orange/brown solid without further purification. ^1H NMR: (500 MHz, DMSO-d_6) δ 8.13 (d, $J=8.39$ Hz, 2H), δ 7.50 (d, $J=8.39$ Hz, 2H), δ 7.38 (s, 1H), δ 7.01 (s, 1H), δ 3.41 (q, $J=3.51$ Hz, $J=4.88$ Hz, 1H), δ 3.02 (dd, $J=8.24$ Hz, $J=5.04$ Hz, 1H), δ 2.76 (dd, $J=8.24$ Hz, $J=5.04$ Hz, 1H) ^{13}C NMR: (125 MHz, DMSO-d_6) δ 176.34, 147.76, 145.41, 130.64, 123.05, 55.91, 40.88.



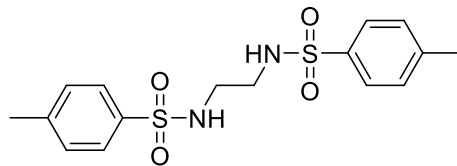
p-NO₂-L-phenylalanine diamine dihydrochloride (**5**)

p-NO₂-L-phenylalanine amide (**4**) (6.21 g, 29.4mmol) was suspended in distilled THF (100 mL) and stirred at -78°C under N₂ atmosphere for 1 hour. To this, 1 M BH₃*THF (150 mL) was slowly added via glass syringe which aided in dissolution. This orange solution was then allowed to continue stirring at -78°C under N₂ atmosphere for 1 hour before bringing to reflux for 16 hours. The, now yellow, solution was then returned to -78°C and dry MeOH (20 mL) was slowly added. Solution was then brought to room temperature, affording H₂(g). Solvent was then removed under reduced pressure, additional MeOH (20 mL) was added, and solvent was again removed under reduced pressure. The resulting residue was then taken up into absolute EtOH (80 mL) to which was bubbled HCl (g) generated from dropwise addition of concentrated H₂SO₄ over NaCl (s) until solution was saturated. The reaction suspension was then set to reflux for 2 hours under N₂ atmosphere. When complete, the reaction was stoppered and placed in a freezer at -15°C overnight. Precipitated diamine dihydrochloride was then isolated via vacuum filtration as a white solid (4.02 g, 50.9%) ¹H NMR: (500 MHz, D₂O) δ 8.26 (d, J=8.85 Hz, 2H), δ 7.61 (d, J=8.85 Hz, 2H), δ 4.07 (p, J=6.87 Hz, 1H), δ 3.44 (m, 2H), δ 3.24 (m, 2H). ¹³C NMR: (125 MHz, D₂O) δ 147.24, 141.98, 130.61, 125.14, 50.28, 43.00, 36.03.



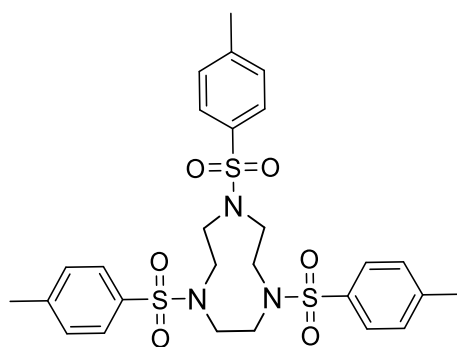
p-NO₂-L-phenylalanine ditosyl diamine (**6**)

p-NO₂-L-phenylalanine diamine dihydrochloride (1.45g, 5.13 mmol) was suspended in dry DCM (50 mL) and set to stir under N₂ atmosphere at 0°C. To this, distilled Et₃N (3.10 mL) was added and aided in dissolution. A solution of tosyl chloride (2.33g, 11.9 mmol), recrystallized from petroleum ether, in DCM (10 mL) was then added dropwise over the course of 30 minutes then fixed with a reflux condenser. Over the course of 16 hours, this solution was brought up to room temperature. The pale-yellow solution was then washed with water (2x100 mL), 1 M HCl (2x100 mL), then finally brine (2x100 mL). The organic layer was then dried with NaSO₄, and the solvent was reduced via vacuum. Recrystallization from dry MeOH then yielded a tan solid (2.41g, 93.1% yield) ¹H NMR: (500 MHz, CDCl₃) δ 7.79 (dd, J=8.59 Hz, 2H), δ 7.75 (d, J=6.44 Hz, 2H) δ 7.40 (d, J=8.30 Hz, 2H), δ 7.27 (d, J=8.10 Hz, 2H), δ 7.03 (d, J=8.68 Hz, 4H), δ 5.93 (t, J=6.64 Hz, 1H), δ 5.84 (d, J=8.20 Hz, 1H) δ 3.52 (m, 1H), δ 3.13 (t, J=5.37 Hz, 2H), δ 2.76 (m, 2H), δ 2.40 (s, 3H), δ 2.33 (s, 3H). ¹³C NMR: (125 MHz, CDCl₃) δ 146.59, 144.91, 143.86, 143.81, 136.72, 136.56, 130.05, 129.95, 129.56, 127.21, 126.83, 123.46, 55.23, 47.48, 38.12, 21.62, 21.40.



N,N'-ditosyl ethylenediamine (**10**)

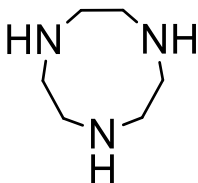
Ethylenediamine (5.47 mL, 81.4 mmol) and distilled Et₃N (24.0 mL) was added to a 1 L round bottom flask containing DCM (250 mL) and set to stir at 0°C for 5 minutes under N₂ atmosphere. To this tosyl chloride (32.6g, 0.170 mol), recrystallized from petroleum ether, was added while continuing to purge N₂. This solution was then set to stir from 0°C to room temperature over 16 hours. Then, ice-cold deionized water (400 mL) was added to the solution forming a white precipitate that was then collected via vacuum filtration. The solid was then redissolved in dry DCM (200 mL) and water with 1 M HCl (2x100 mL) and brine (2x100 mL). The solution was dried using Na₂SO₄ and solvent was removed under reduced pressure to yield a white solid (27.2g, 90.9% yield) ¹H NMR: (500 MHz, CDCl₃) δ 7.70 (d, J=8.24 Hz, 4H), δ 7.32 (d, J=8.24 Hz, 4H), δ 4.81 (s, 2H), δ 3.05 (s, 2H), δ 2.43 (s, 6H).



N,N',N''-tritosyl triazacyclononane (**11**)

Cesium carbonate (18.7g, 57.3 mmol) was suspended in dry DMF (500 mL) and set to stir at room temperature for 15 minutes under N₂ atmosphere in a 2 L 3-neck round bottom flask.

To this, **(10)** (10.0g, 27.1 mmol) was added, fitted with a reflux condenser, and set to stir for 60 minutes at 100°C. Then a solution of **(8)** (17.8 g, 31.3 mmol) in dry DMF (250 mL) was added dropwise over the course of 2 hours. This was allowed to continue stirring at 100°C under N₂ atmosphere for 24 hours then a further 24 hours at room temperature. To this solution, ice-cold deionized water (500 mL) was added causing precipitation of a white solid that was collected via vacuum filtration. The collected solid was then redissolved in dry DCM (250 mL) and washed with water (2x100 mL), 1 M HCl (2x100 mL), and brine (2x100 mL). This pale-yellow solution was then dried using Na₂SO₄ and solvent was removed under reduced pressure to yield an off-white solid (12.2g, 66.2% yield). ¹H NMR: (500 MHz, CDCl₃) δ 7.68 (d, J=8.24 Hz, 6H), δ 7.32 (d, J=8.09 Hz, 6H), δ 3.41 (s, 12H), δ 2.41 (s, 9H). ¹³C NMR: (125 MHz, CDCl₃) δ 143.98, 134.68, 129.96, 127.57, 51.93, 21.60.



Triazacyclononane (12)

N,N',N''-tritosyl triazacyclononane (10.0, 16.9 mmol) was dissolved in concentrated H₂SO₄ (60 mL), fitted with a reflux condenser, and set to stir at 100°C under N₂ atmosphere for 3 days. Solution was the brought to 0°C and absolute EtOH (60 mL) that had been previously cooled to 0°C was added dropwise while maintaining stirring. Then, Et₂O (100 mL) that had also been chilled was added dropwise and resulted in a black precipitate which was collected via vacuum filtration. This was then dissolved in minimum H₂O and pH was adjusted to 14 using

NaOH pellets and extracted into CHCl_3 (5x50 mL). Solution was then dried over Na_2SO_4 , and solvent was removed under reduced pressure to yield a white solid. ^1H NMR: (500 MHz, CDCl_3) δ 2.77 (s, 12H), δ (s, 3H). ^{13}C NMR: (125 MHz, CDCl_3) δ 47.73.

List of References

1. Goldenberg DM, Sharkey RM. Advances in cancer therapy with radiolabeled monoclonal antibodies. *Q. J. Nucl. Med. Mol. Imaging*. **2006**; *50*: 248–64.
2. Goldenberg DM, Sharkey RM. Novel radiolabeled antibody conjugates. *Oncogene*. **2007**; *26*: 3734–44.
3. McCardle RJ, Harper PV, Spar IL, Bale WF, Andros G, Jiminez F. Studies with iodine-131-labeled antibody to human fibrinogen for diagnosis and therapy of tumors. *J. Nucl. Med.* **1966**; *7*: 837–47.
4. Zhang Y, Hong H, Cai W. PET tracers based on Zirconium-89. *Curr Radiopharm.* **2011**; *4* (2): 131–9.
5. Shukla AK, Kumar U. Positron emission tomography: An overview. *J Med Phys.* **2006**, *31*: 13–21.
6. Pearson, R. Hard and Soft Acids and Bases. *J. Am. Chem. Soc.* **1963**, *85* (22): 3533–3539
7. Shannon, R.; Prewitt, C.T. *Acta Crystallogr.* **1969**, *B25*, 925
8. Hancock, D. R. *Inorg. Chem.* **1990**, *29*, 1968-1974
9. Dayani, P. N. Desferoxamine (DFO)--mediated iron chelation: rationale for a novel approach to therapy for brain cancer. *J. Neurooncol.* **2004**, *67* (3): 366-367
10. Grime, Stefan. Semiempirical Hybrid Density Functional with Perturbative Second-Order Correlation. *J. Chem. Phys.* **2006**. *124* (3)
11. Louie, S. G.; Froyen, S.; Cohen, M. L., Nonlinear ionic pseudopotentials in spin-density-functional calculations, *Phys. Rev. B*, **1986**, *26* (4): 1738–1742.
12. Jensen, F. Atomic orbital basis sets. *WIREs Comput. Mol. Sci.* **2013**. *3* (3): 273–295.
13. Alauddin M. M. Positron emission tomography (PET) imaging with ¹⁸F-based radiotracers. *Am. J. Nucl. Med. Mol.* **2012**, *2*, 55–76.
14. Breeman, W. A.; de Blois, E.; Sze Chan, H.; Konijnenberg, M.; Kwekkeboom, D. J.; Krenning, E. P. ⁶⁸Ga-labeled DOTA-peptides and ⁶⁸Ga-labeled radiopharmaceuticals for positron emission tomography: current status of research, clinical applications, and future perspectives. *Semin. Nucl. Med.* **2011**, *41*, 314–21.
15. Roesch, F.; Riss, P. J. The renaissance of the ⁶⁸Ge/⁶⁸Ga radionuclide generator initiates new developments in ⁶⁸Ga radiopharmaceutical chemistry. *Curr. Top. Med. Chem.* **2010**, *10*, 1633–68.

16. Anderson, C. J.; Ferdani, R. Copper-64 radiopharmaceuticals for PET imaging of cancer: Advances in preclinical and clinical research. *Cancer Biother. Radiopharm.* **2009**, *24*, 379–393.
17. Ferguson, S., Jans, HS., Wuest, M. *et al.* Comparison of scandium-44 g with other PET radionuclides in pre-clinical PET phantom imaging. *EJNMMI Phys.* **2019**, *6*, 23.
18. Kolsky, K. L.; Joshi, V.; Mausner, L. F.; Srivastava, S. C. Radiochemical purification of no-carrier-added scandium-47 for radioimmunotherapy. *Appl. Radiat. Isot.* **1998**, *49*, 1541–9.
19. Koumariou, E.; Loktionova, N. S.; Fellner, M.; Roesch, F.; Thews, O.; Pawlak, D.; Archimandritis, S. C.; Mikolajczak, R. ⁴⁴ScDOTA-BN[2-14]NH₂ in comparison to ⁶⁸Ga-DOTA-BN[2-14]NH₂ in pre-clinical investigation. Is ⁴⁴Sc a potential radionuclide for PET? *Appl. Radiat. Isot.* **2012**, *70*, 2669–76.
20. Hernandez R., Valdovinos H.F., Yang Y., Chakravarty R., Hong H., Barnhart T.E., Cai W.; ⁴⁴Sc: An attractive isotope for Peptide-Based PET Imaging. *Mol.Pharm.* **2014**. *11*. (8), 2954-2961.
21. Filosofov, D. V.; Loktionova, N. S.; Roesch, F. A ⁴⁴Ti/⁴⁴Sc radionuclide generator for potential nuclear-medical application of ⁴⁴Sc-based PET-radiopharmaceuticals. *Radiochim. Acta*, **2010**, *98*, 149– 156. (29)
22. Severin, G. W.; Engle, J. W.; Valdovinos, H. F.; Barnhart, T. E.; Nickles, R. J. Cyclotron produced ^{44g}Sc from natural calcium. *Appl. Radiat. Isot.* **2012**, *70*, 1526–30.
23. Huclier-Markai S., Kerdjoudj R., Alliot C., Bonraisin A.C., Michel N., Haddad F., Barbet J.; Optimizations of Reaction Conditions for the Radiolabeling of DOTA and DOTA-Peptide with ^{44m/44g}Sc and Experimental Evidence of the feasibility of an *in vivo* PET Generator. *Nuc. Med. Bio.* **2014**, *41*, 36-43.
24. Drahos B., Kubicek V., Bonnet C. S., Hermann P., Lukes I. Toth E.; Dissociation Kinetics of Mn²⁺ complexes of NOTA and DOTA. *Dalton Trans.*, **2011**, *40*, 1945–1951.
25. Sibbons, K.F.; Shastri, K.; Watkinson, M.; The application of manganese complexes of ligands derived from 1,4,7-triazacyclononane in oxidative catalysis. *Dalton Transactions.* (2006), (5): 645–661.
26. Deal, K.A.; Burstyn, J.N. Mechanistic Studies of Dichloro(1,4,7-triazacyclononane) copper(II)-Catalyzed Phosphate Diester Hydrolysis. *Inorg. Chem.* (1996), *35* (10): 2792–2798.

27. Wieghardt, K.; Schmidt, W.; Hermann, W.; Küppers, H.-J. Redox potentials of bis(1,4,7-triazacyclononane) complexes of some first transition series metals(II,III). Preparation of bis(1,4,7-triazacyclononane) nickel(III) perchlorate. *Inorg. Chem.* (1983), 22 (20): 2953.
28. Chan, T. H.; Huang, J.; Zhou, Z. An Improved Synthesis of 1,4,7-Triazacyclononanes (Tacns) and 1,4,7,10-Tetraazacyclododecanes (Cyclens). *Synthesis* 2009, 14, 2341–44.
29. Schwarzenbach G. "Der Chelateffekt" [The Chelation Effect]. *Helvetica Chimica Acta.* 1952. 35 (7): 2344–59.
30. Sdsd
31. Richman, J. E.; Atkins, T. J. Nitrogen Analogs of Crown Ethers. *J. Am. Chem. Soc.*, 1974, 96 (7), 2268–2270.
32. Pandya D.N., Bhatt N., Yuan H., Day C.S., Ehrmann B.M., Wright M., Bierbach U., Wadas T.J. Zirconium tetraazamacrocyclic complexes display extraordinary stability and provide a new strategy for zirconium-89-based radiopharmaceutical development. *Chem. Sci.* 2017, 8:2309–14.
33. Price, E.W., Orvig, C.; Matching Chelators to Radiometals for Radiopharmaceuticals. *Chem. Soc. Rev.*, 2014, 43, 260–290.
34. Deri, M.A., Ponnala, S., Kozlowski, P., Burton-Pye, B.P., Cicek, H.T., Hu, C., Lewis, J.S., Francesconi, L.C.; *Bioconjugate Chem.*, 2015, 26, 2579–2591.
35. Deri, M.A., Ponnala, S., Zeglis, B.M., Pohl, G., Dannenberg, J.J., Lewis, J.S., Francesconi; Alternative Chelator for ⁸⁹Zr Radiopharmaceuticals: Radiolabeling and Evaluation of 3,4,3-(LI-1,2-HOPO) *J. Med. Chem.*, 2014, 57, 4849–4860.
36. E. Boros, J. P. Holland, N. Kenton, N. Rotile and P. Caravan, *ChemPlusChem*, 2016, 81, 274–281.
37. F. Guerard, Y. S. Lee, R. Tripier, L. P. Szajek, J. R. Deschamps and M. W. Brechbiel, *Chem. Commun.*, 2013, 49, 1002–1004.
38. F. Guerard, Y.-S. Lee and M. W. Brechbiel, *Chem.–Eur. J.*, 2014, 20, 5584–5591.
39. O. Jacobson, L. Zhu, G. Niu, I. D. Weiss, L. P. Szajek, Y. Ma, X. Sun, Y. Yan, D. O. Kiesewetter, S. Liu and X. Chen, *Mol. Imaging Biol.*, 2011, 13, 1224–1233.
40. M. T. Ma, L. K. Meszaros, B. M. Paterson, D. J. Berry, M. S. Cooper, Y. Ma, R. C. Hider and P. J. Blower, *Dalton Trans.*, 2015, 44, 4884–4900.

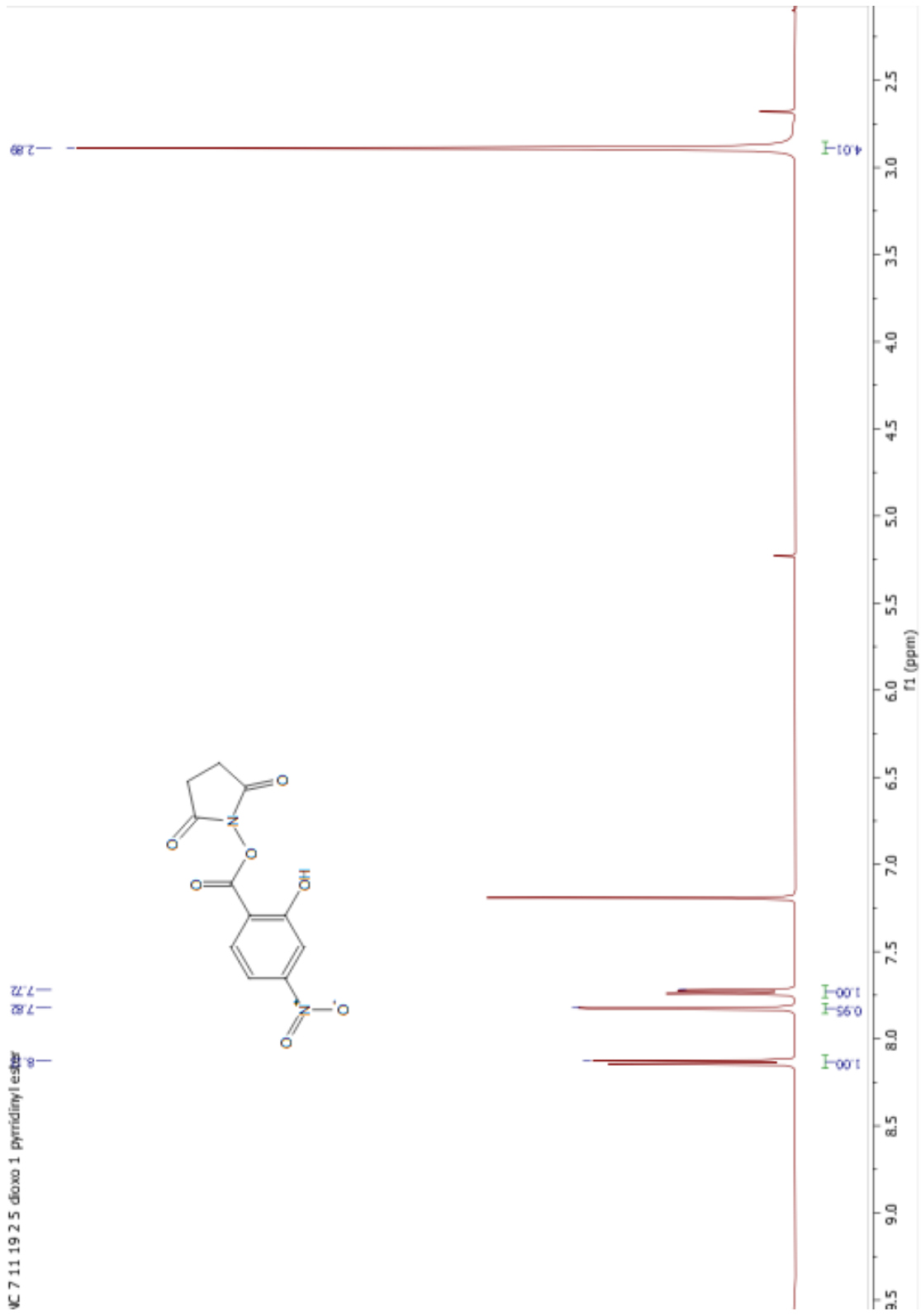
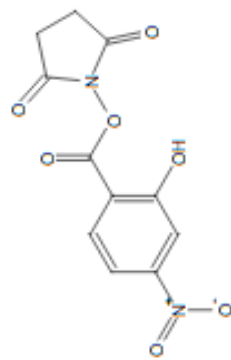
41. D. N. Pandya, S. Pailloux, D. Tatum, D. Magda and T. J. Wadas, *Chem. Commun.*, 2015, 51, 2301–2303.
42. M. Patra, A. Bauman, C. Mari, C. A. Fischer, O. Blacque, D. Haussinger, G. Gasser and T. L. Mindt, *Chem. Commun.*, 2014, 50, 11523–11525.
43. E. W. Price, B. M. Zeglis, J. S. Lewis, M. J. Adam and C. Orvig, *Dalton Trans.*, 2014, 43, 119–131.
44. V. Radchenko, S. Busse and F. Roesch, *Nucl. Med. Biol.*, 2014, 41, 721–727.
45. J. N. Tinianow, D. N. Pandya, S. L. Pailloux, A. Ogasawara, A. N. Vanderbilt, H. S. Gill, S.-P. Williams, T. J. Wadas, D. Magda and J. Marik, *Theranostics*, 2016, 6, 511–521.
46. F. C. van de Watering, M. Rijpkema, L. Perk, U. Brinkmann, W. J. Oyen and O. C. Boerman, *BioMed Res. Int.*, 2014, 2014, 203601.
47. D. J. Vugts, C. Klaver, C. Sewing, A. J. Poot, K. Adamzek, S. Huegli, C. Mari, G. W. Visser, I. E. Valverde, G. Gasser, T. L. Mindt and G. A. van Dongen, *Eur. J. Nucl. Med. Mol. Imaging*, 2016
48. R. Ferdani, D. J. Stigers, A. L. Fiamengo, L. Wei, B. T. Li, J. A. Golen, A. L. Rheingold, G. R. Weisman, E. H. Wong.
49. Huskens, J.; Sherry, A. D., Synthesis and Characterization of 1,4,7-Triazacyclononane Derivatives with Methylphosphinate and Acetate Side Chains for Monitoring Free Mg^{II} by ³¹P and ¹H NMR Spectroscopy. *J. Am. Chem. Soc.* **1996**, *118* (18), 4396-4404.
50. D. Parker , K. Pulukkody , F. C. Smith , A. Batsanov and J. A. K. Howard, Structures of the yttrium complexes of 1,4,7,10-tetraazacyclododecane-*N,N',N'',N'''*-tetraacetic acid (H₄dota) and *N,N'''*-bis(benzylcarbamoylmethyl)diethylenetriamine-*N,N',N''*-triacetic acid and the solution structure of a zirconium complex of H₄dota, *Dalton Trans.*, **1994**, 689 —93.
51. Massing, J. O. Design, synthesis, and speciation of bifunctional ligands: towards ratiometric fluorescent metal-ion sensing. *UNH Dissertation*. **2013**, 162-4.
52. Dilworth JR, Pascu SI. The chemistry of PET imaging with zirconium-89. *Chemical Society Reviews* **2018**. *47* (8): 2554–71.
53. Meijs W.E., Herscheid J.D.M., Haisma H.J., Pinedo H.M. Evaluation of desferal as a bifunctional chelating agent for labeling antibodies with Zr-89. *Appl. Radiat. Isot.* **1992**; *43*:1443–7.

54. Zeglis BM, Lewis JS. The bioconjugation and radiosynthesis of ^{89}Zr -DFO-labeled antibodies. *J Vis Exp.* **2015**; 96: 52521–8.
55. Zweit, J., Downey, S., Sharma, H.L.; Production of no-carrier-added zirconium-89 for positron emission tomography. *Int. J. Radiat. Appl. Instrum., A, Appl. Radiat. Isot.* **1991**, 42:199–201.
56. Nayak, T.K., Brechbiel, M.W.; Radioimmunoimaging with longer-lived positron-emitting radionuclides: potentials and challenges. *Bioconjug. Chem.* **2009**, 20: 825–841.
57. Holland JP, Divilov V, Bander NH, Smith-Jones PM, Larson SM, Lewis JS, et al. Zr-DFO-J591 for immunoPET imaging of prostate-specific membrane antigen (PSMA) expression in vivo. *J Nucl Med.* **2010**; 51: 1293–300.
58. Abou DS, Ku T, Smith-Jones PM. In vivo biodistribution and accumulation of ^{89}Zr in mice. *Nucl Med Biol.* **2011**; 38: 675–81.
59. Bhatt N.B., Pandya D.N., Wadas T.J. Recent Advances in Zirconium-89 Chelator Development. *Molecules.* **2018**; 23
60. Melson, GA. *Coordination Chemistry of Macrocyclic Compounds.* **1979**. New York: Plenum Press. p. 166.
61. Majkowska-Pilip A, Bilewicz A. Macrocyclic complexes of scandium radionuclides as precursors for diagnostic and therapeutic radiopharmaceuticals. *J Inorg Biochem.* **2011**; 105(2):313-20.
62. Allott L, et al. Evaluation of DFO-HOPO as an octadentate chelator for zirconium-89. *Chem. Comm.* **2017**; 53:8529–32.
63. Zaidi, H., Rahmim, A. PET versus SPECT: strengths, limitations, and challengers. *Nucl. Med. Commun.* **2008**. 29:193-207.
64. Wawrzyniak, N., Suliburska, J.; Nutritional and health factors affecting the bioavailability of calcium: a narrative review. *Nutr Rev.* **2021**; 79: 1307-1320.
65. Pelletier, S. W., *Chem. Ind.* (London) **1953**, 1034.

APPENDIX

VC 7 11 19 2 5 dioxo 1 pyridinyl ester

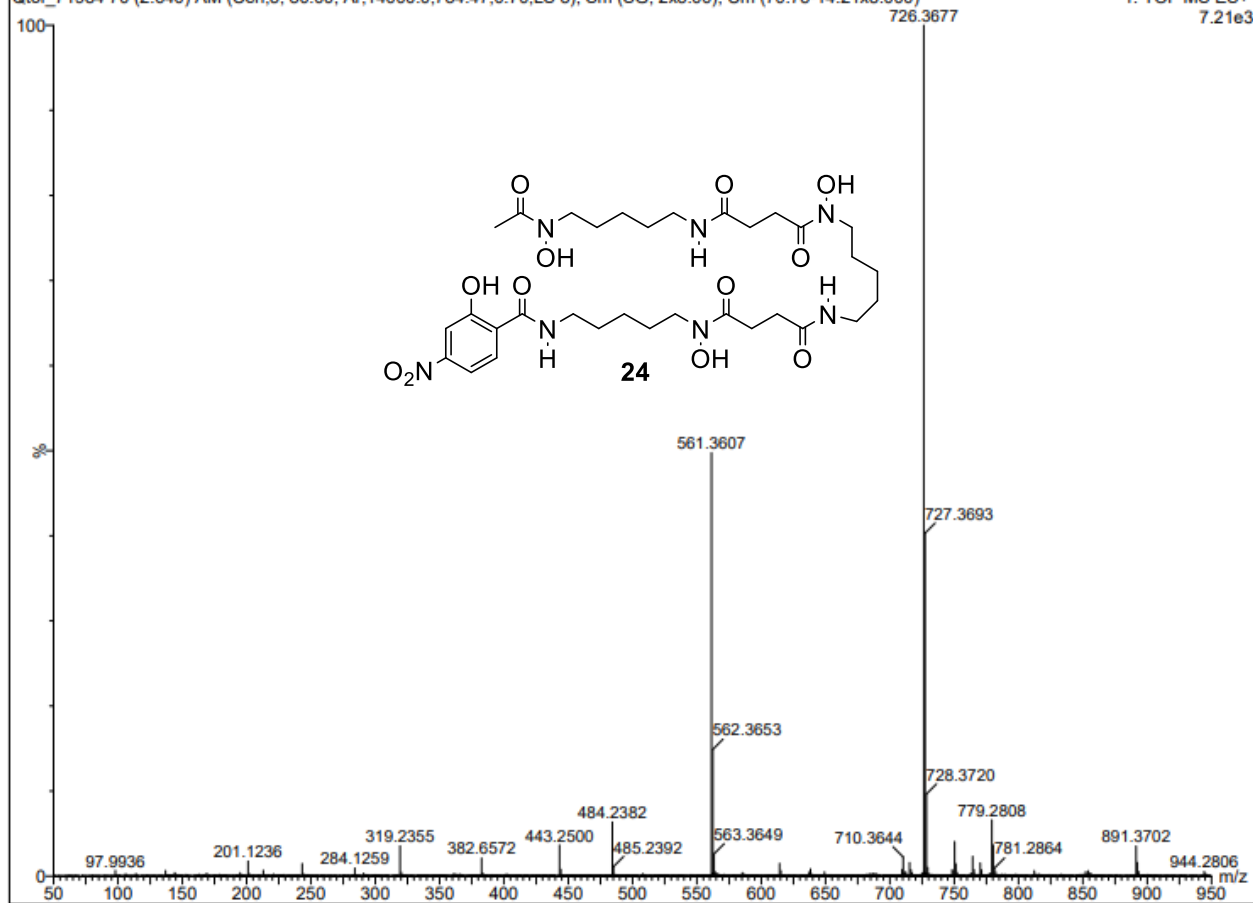
7.72
7.78
7.8

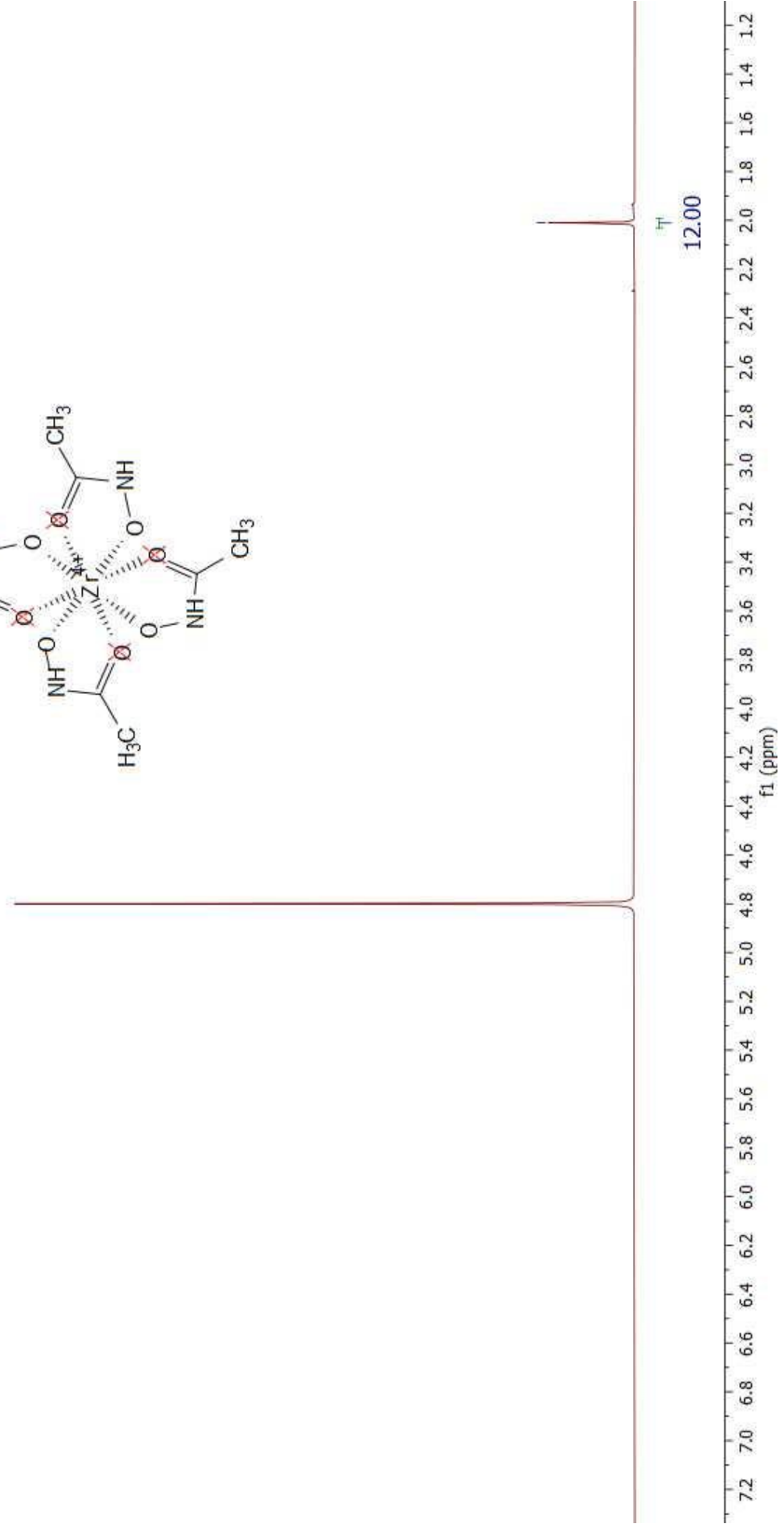
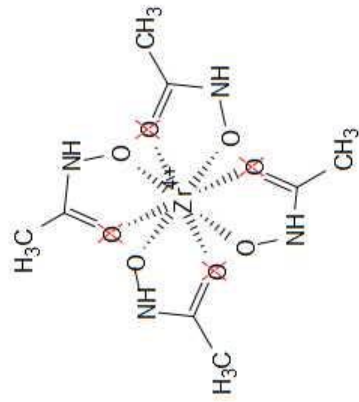


NC1-26

Qtof_71984 70 (2.640) AM (Cen,5, 80.00, Ar,14000.0,734.47,0.70,LS 5); Sm (SG, 2x5.00); Cm (70:75-14:21x8.000)

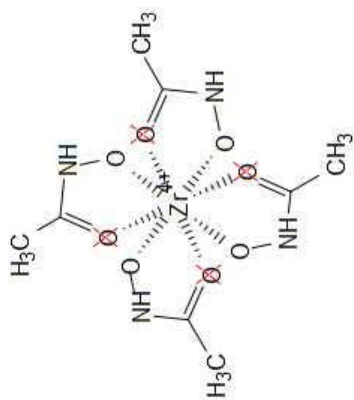
1: TOF MS ES+
7.21e3



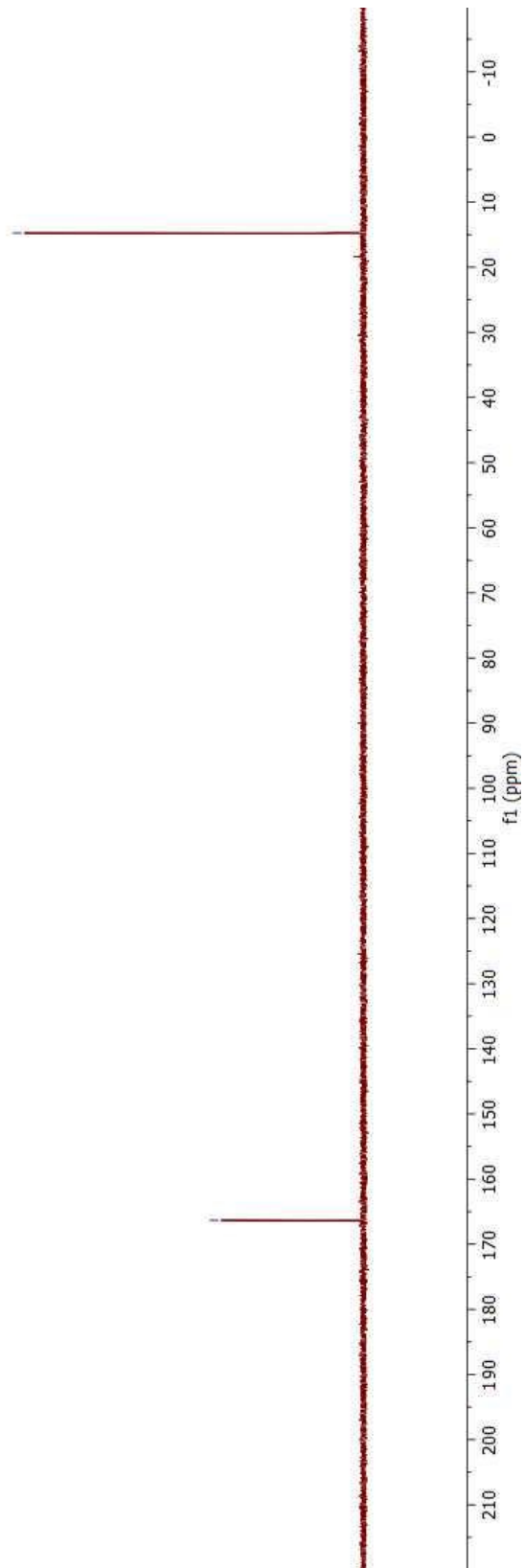


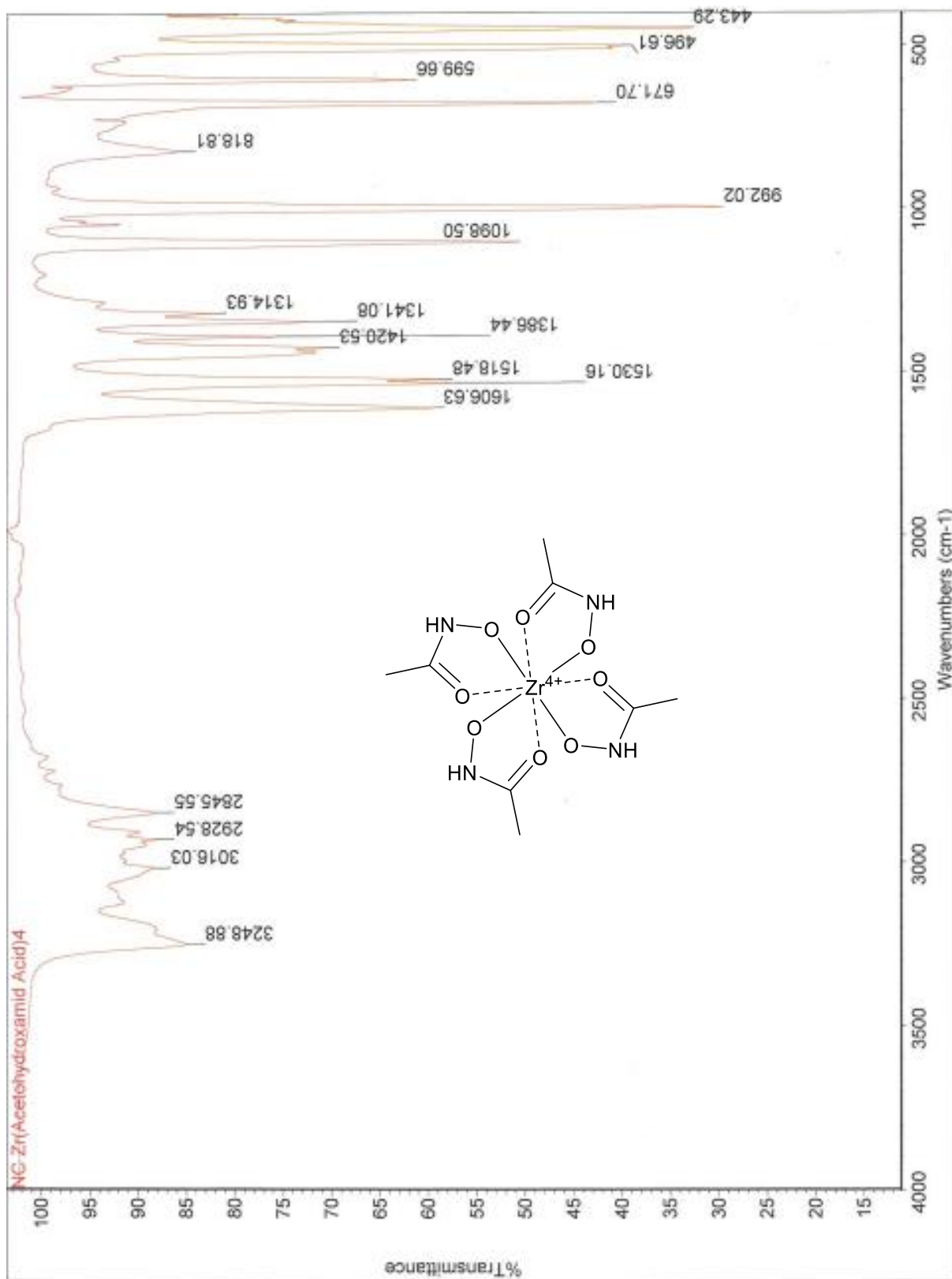
ip-noah Zr(AH).11.fid
Cl3CPD D2O /opt/data nmrsu 16

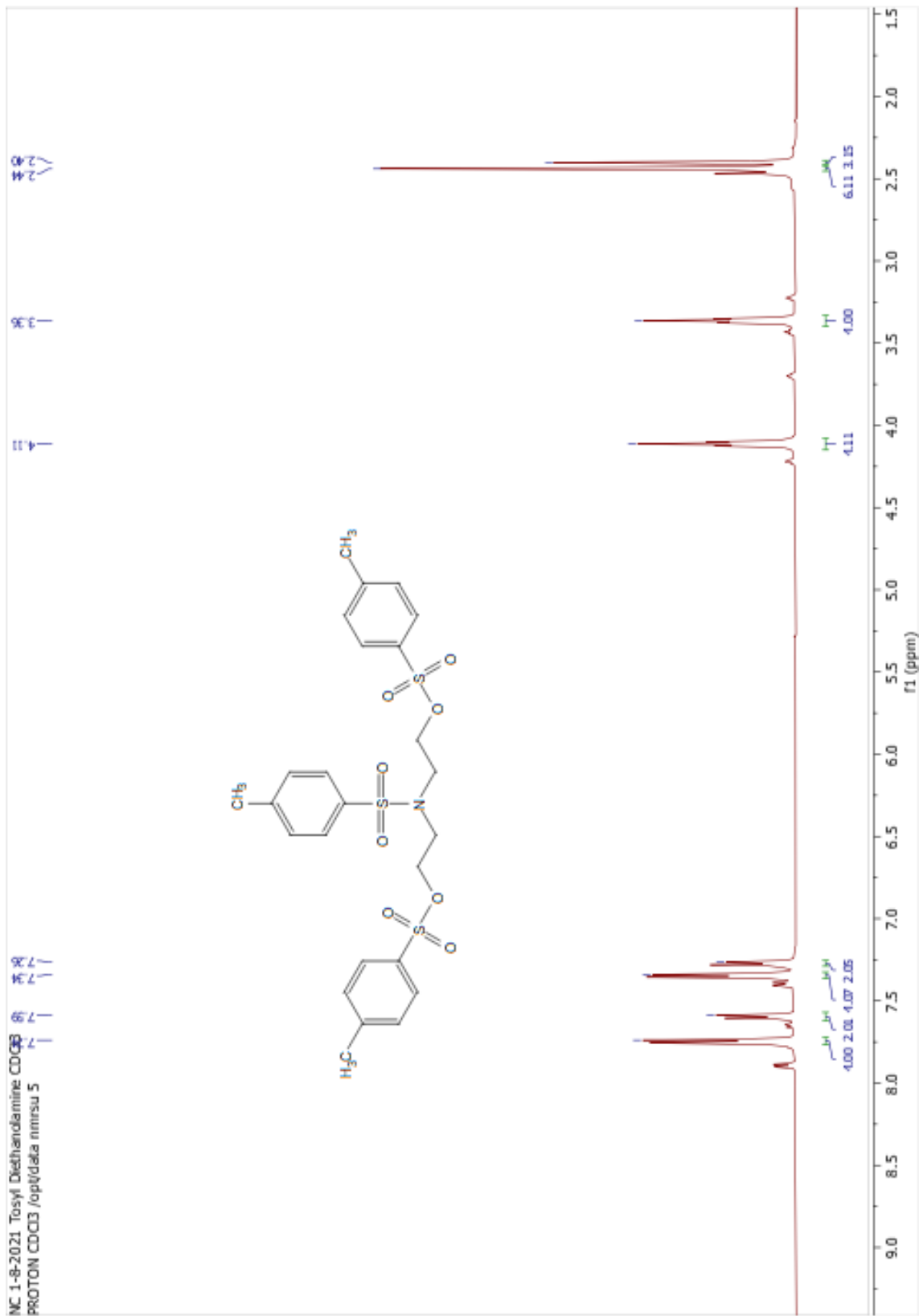
— 166.32



— 14.75







MC_1-8-2021_Tosyl_Diethandamine_CDCl3
C13CPD CDCl3 /opt/data/nmr/su 5

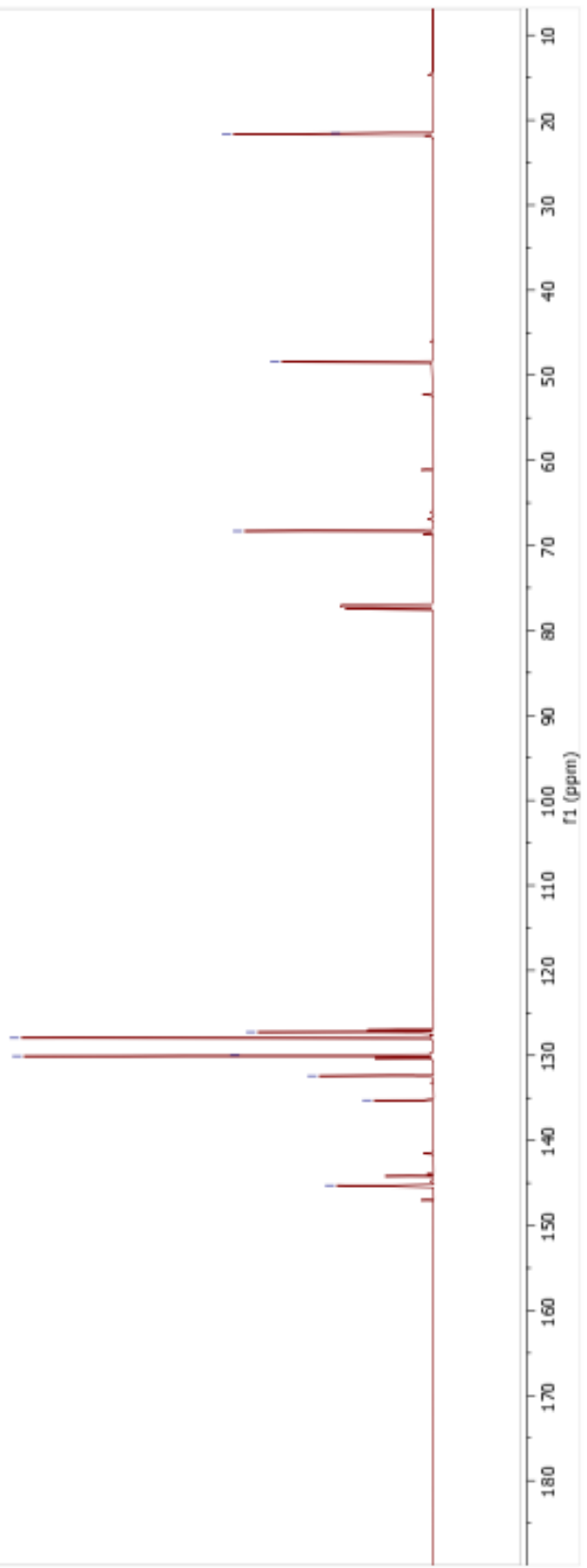
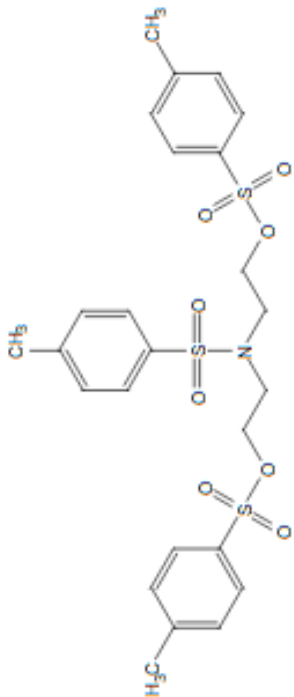
127.74
127.72
127.69
127.67
127.65
127.63
127.61

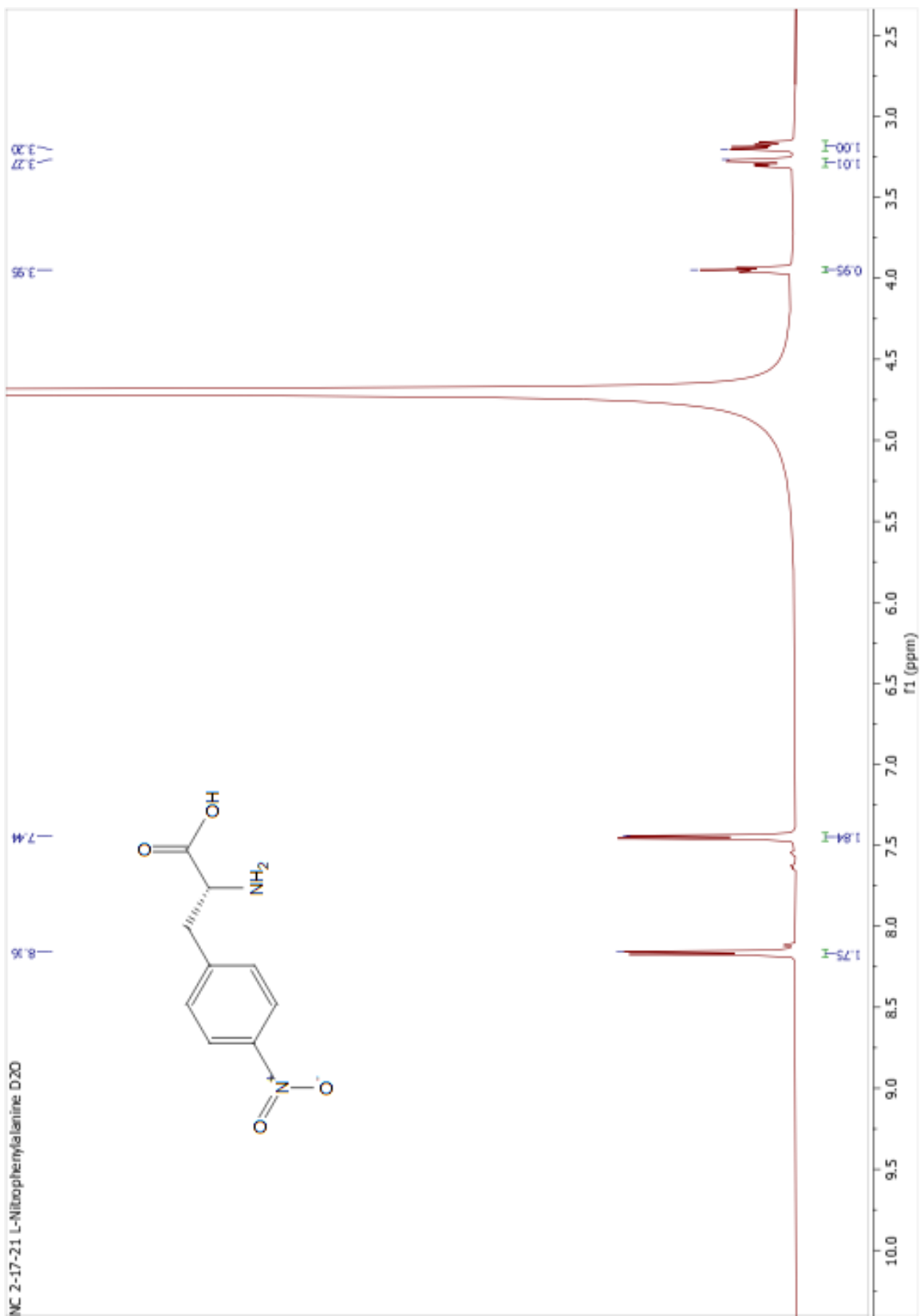
1.66

21.68
21.54

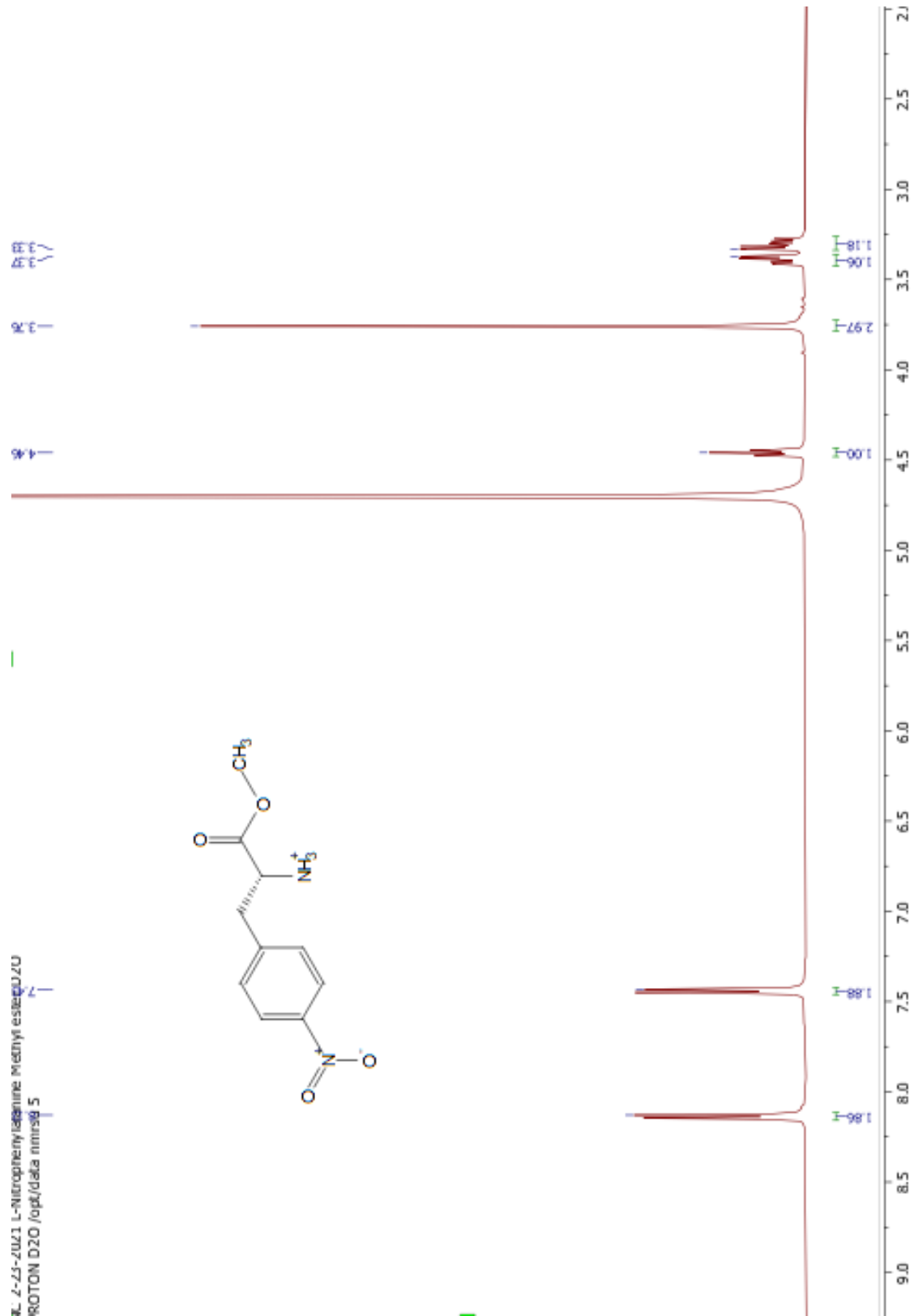
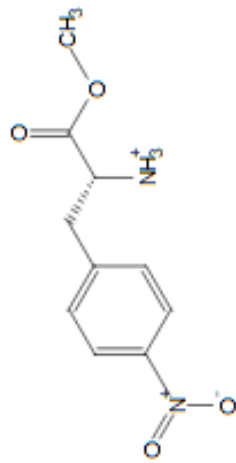
48.45

68.33

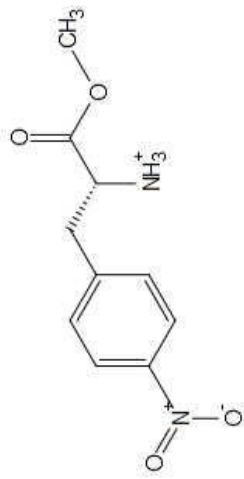




K. 2-25-2021 L-Nitrophenylalanine Methyl ester.p20
ROTON D2O /opt/data/nmr5g_5



NC 4-19-2021 L-Nitrophenylalanine Methyl Ester D2O
Cl3CPD D2O /opt/topspin4.0.7 nmrsu 1



35.29

53.51
53.62

123.96

130.48

141.87

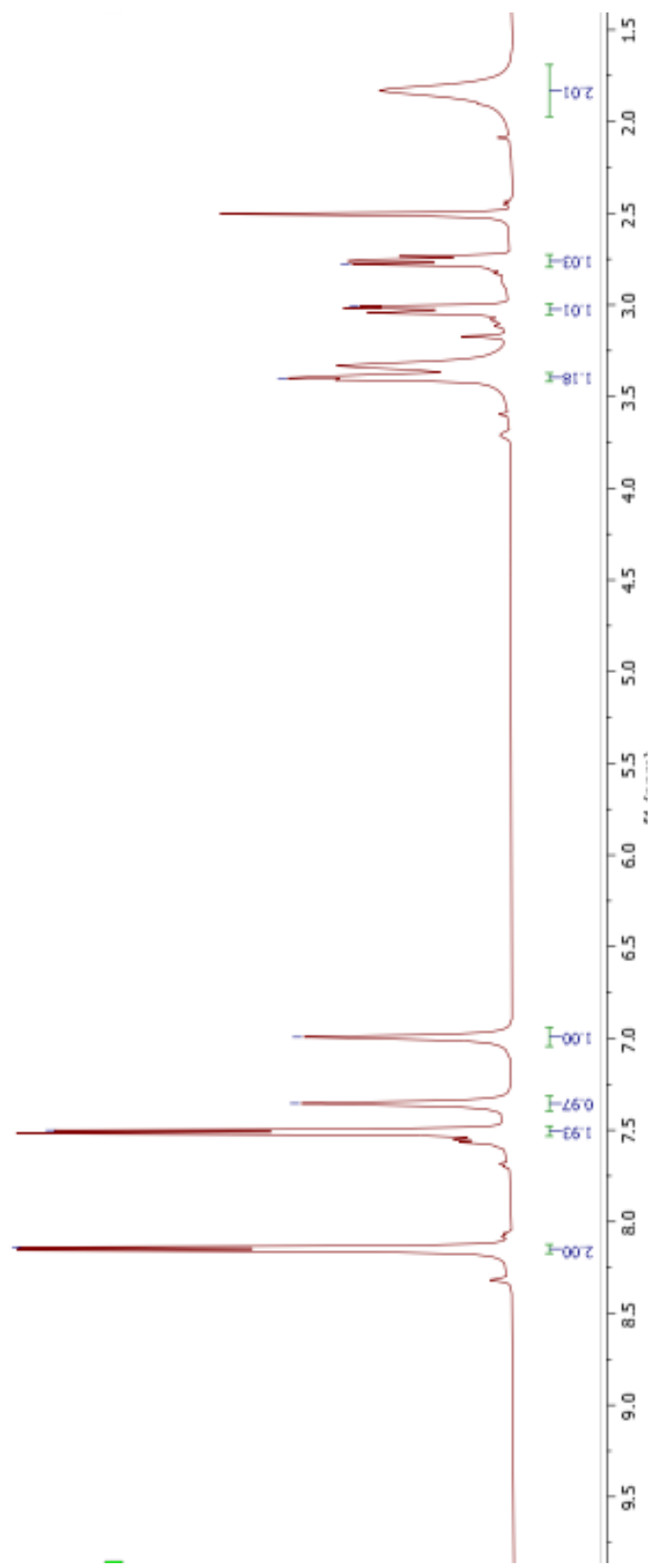
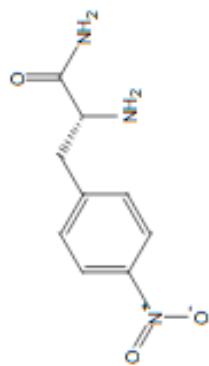
147.22

169

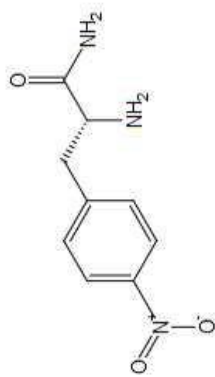
210 200 190 180 170 160 150 140 130 120 110 100 90 80 70 60 50 40 30

f1 (ppm)

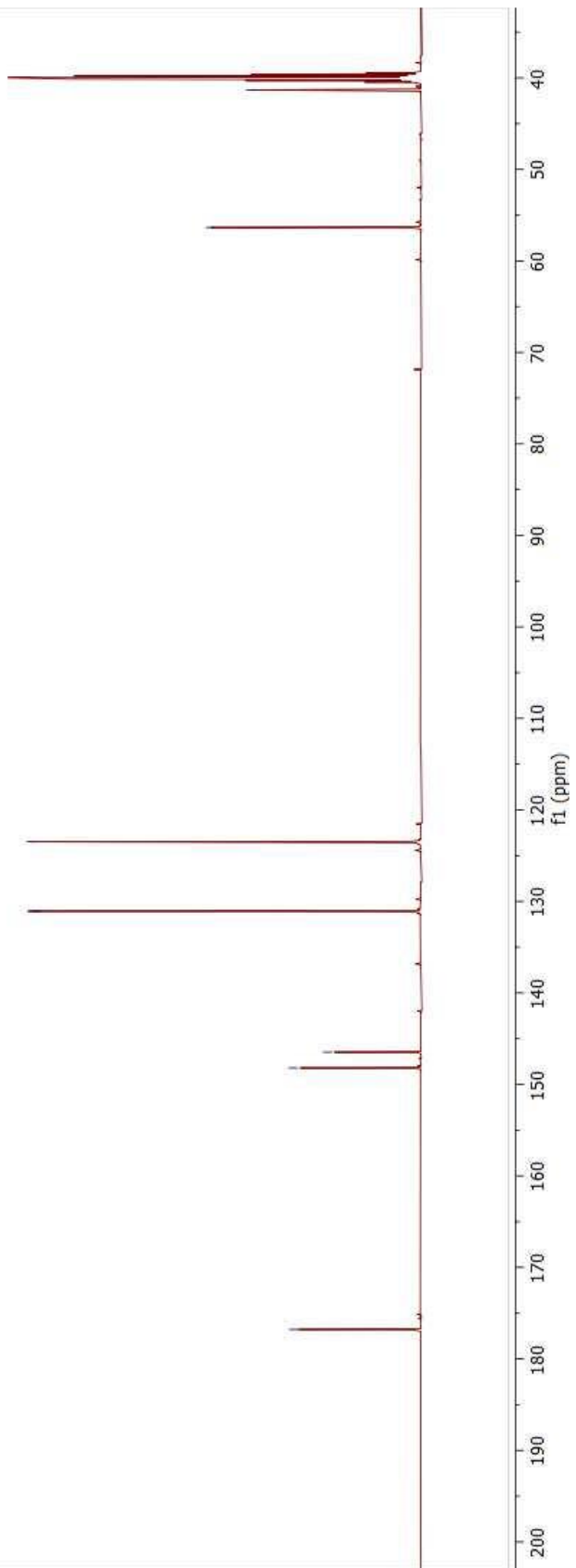
1H NMR spectrum of L-Nitrophenylalanine amide 3-22-2021 DMSO-d6
Peak list (ppm): 8.1, 7.9, 7.7, 7.6, 7.5, 7.4, 7.3, 7.2, 7.1, 7.0, 6.9, 6.8, 6.7, 6.6, 6.5, 6.4, 6.3, 6.2, 6.1, 6.0, 5.9, 5.8, 5.7, 5.6, 5.5, 5.4, 5.3, 5.2, 5.1, 5.0, 4.9, 4.8, 4.7, 4.6, 4.5, 4.4, 4.3, 4.2, 4.1, 4.0, 3.9, 3.8, 3.7, 3.6, 3.5, 3.4, 3.3, 3.2, 3.1, 3.0, 2.9, 2.8, 2.7, 2.6, 2.5, 2.4, 2.3, 2.2, 2.1, 2.0, 1.9, 1.8, 1.7, 1.6, 1.5, 1.4, 1.3, 1.2, 1.1, 1.0, 0.9, 0.8, 0.7, 0.6, 0.5, 0.4, 0.3, 0.2, 0.1, 0.0

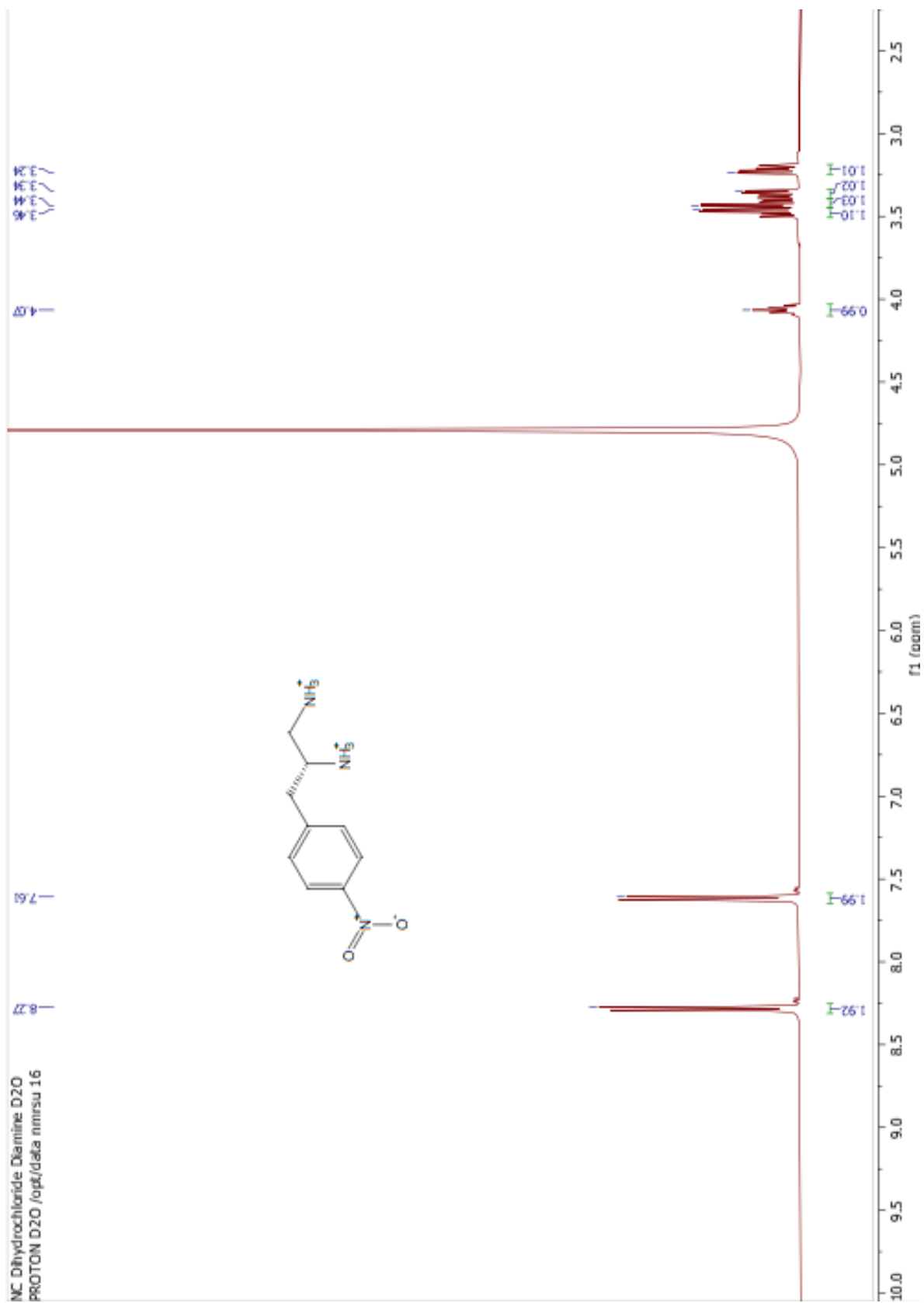


NC-4-7-2021 L-Nitrophenylalagine Amide DMSO d6
Cl3CPD DMSO /opt/data/nmr/22



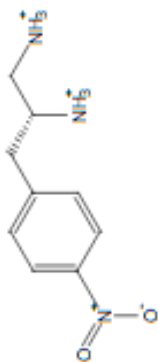
148.20
146.47
131.08
123.48
56.35
41.31





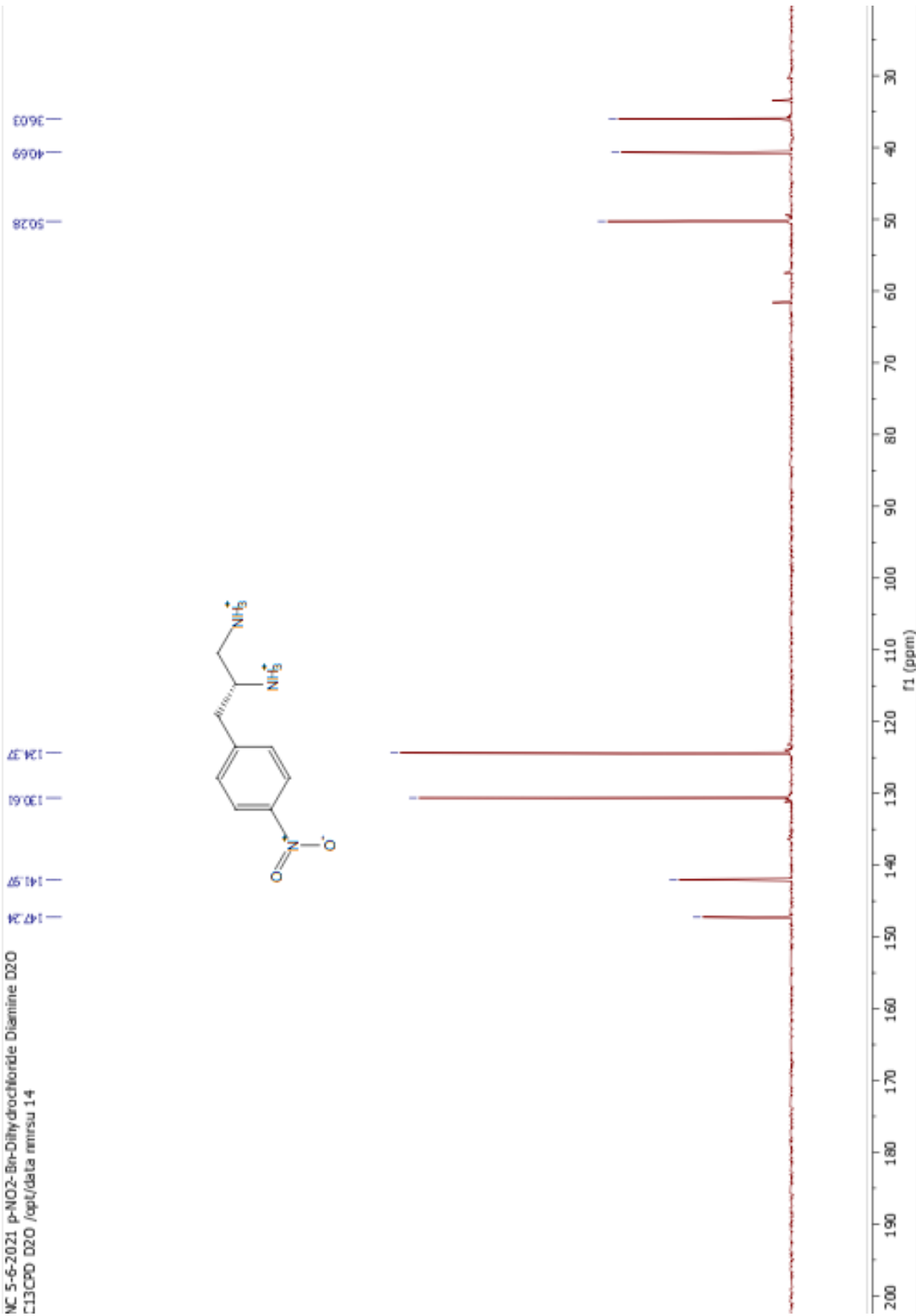
NC 5-6-2021 p-NO2-Br-Diethylchloride Diamine D2O
C13CPD D2O /opt/data renisu 14

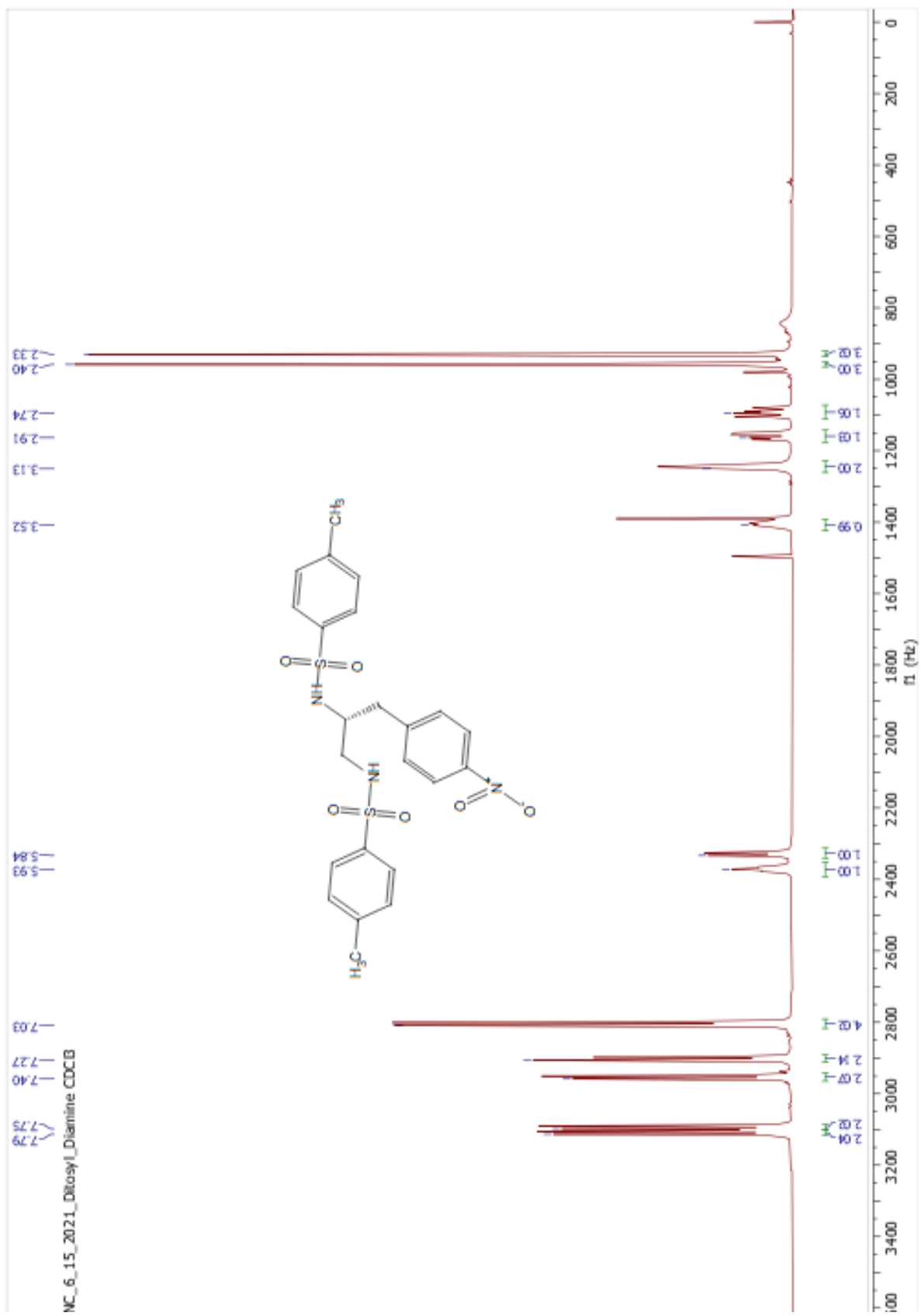
5028
4069
3603

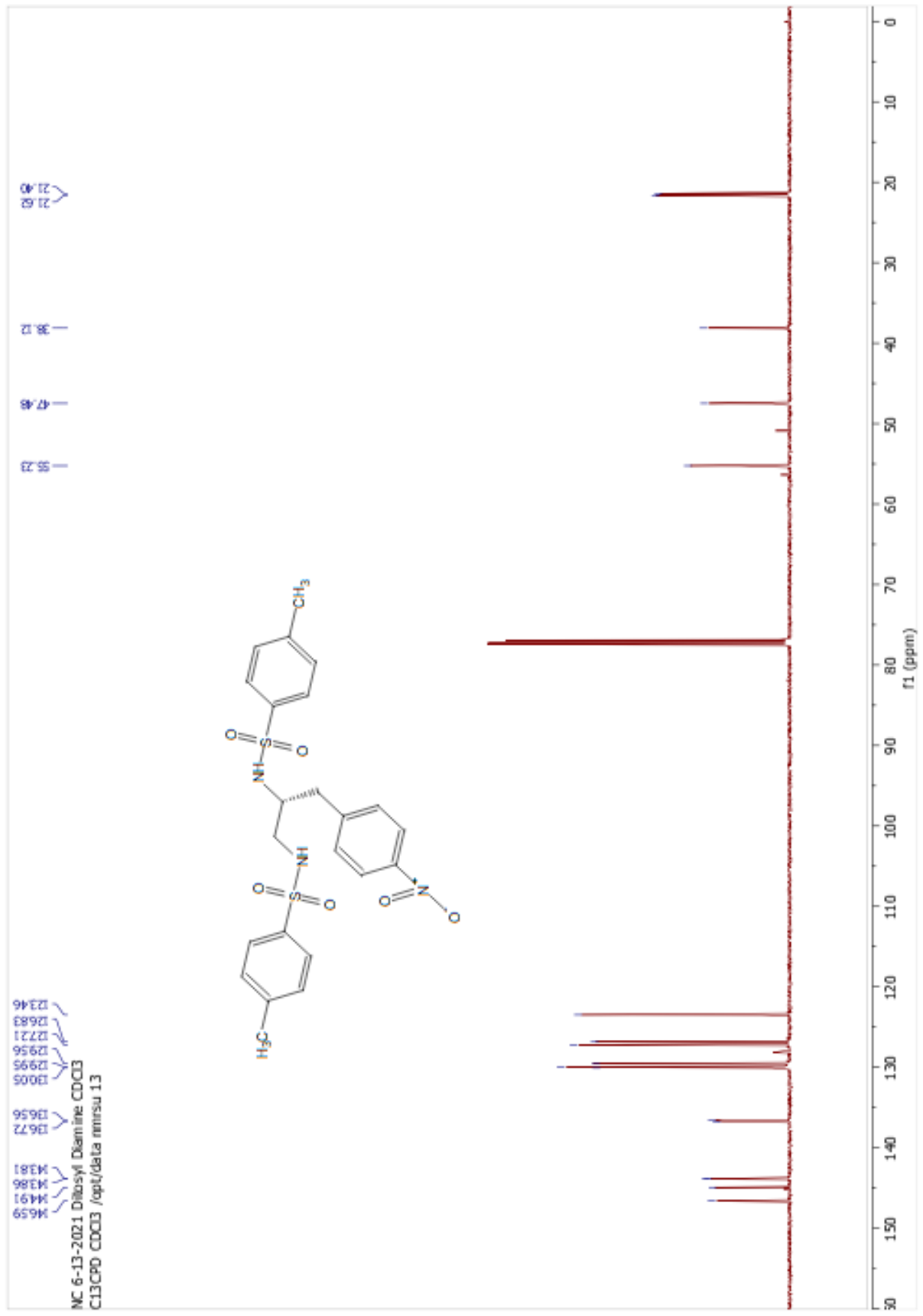


127.1
130.1
131.1
141.97

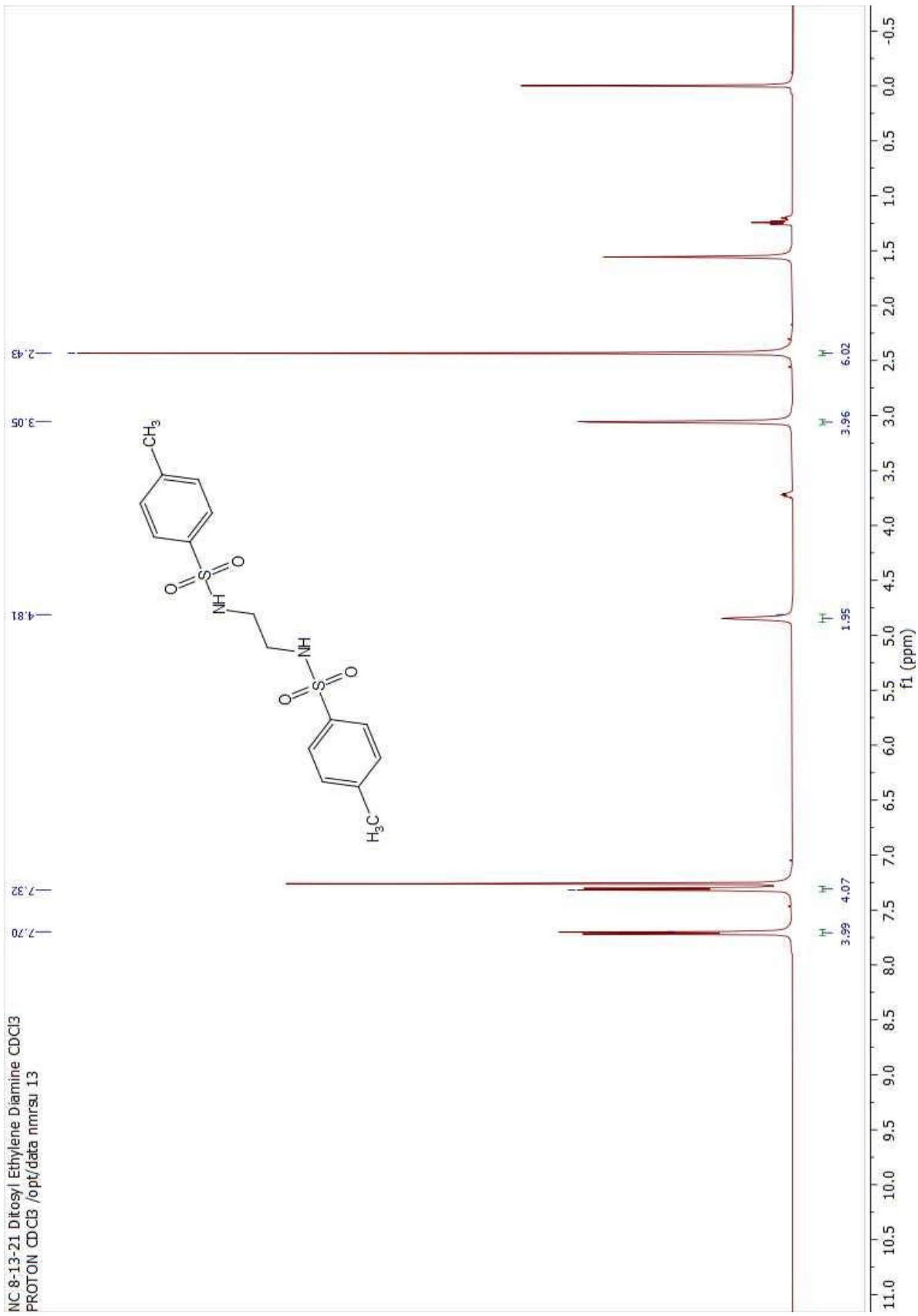
127.1
130.1



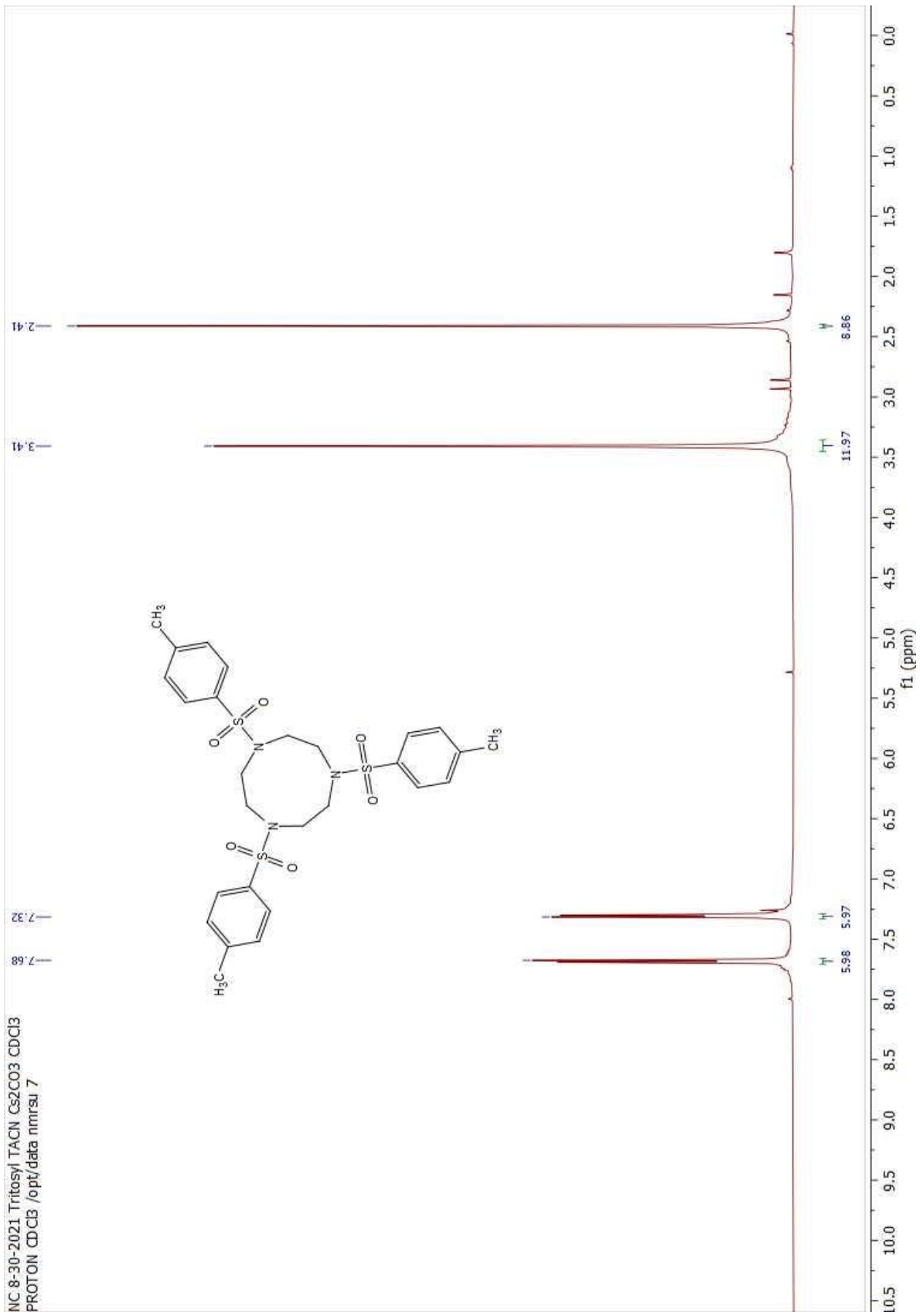


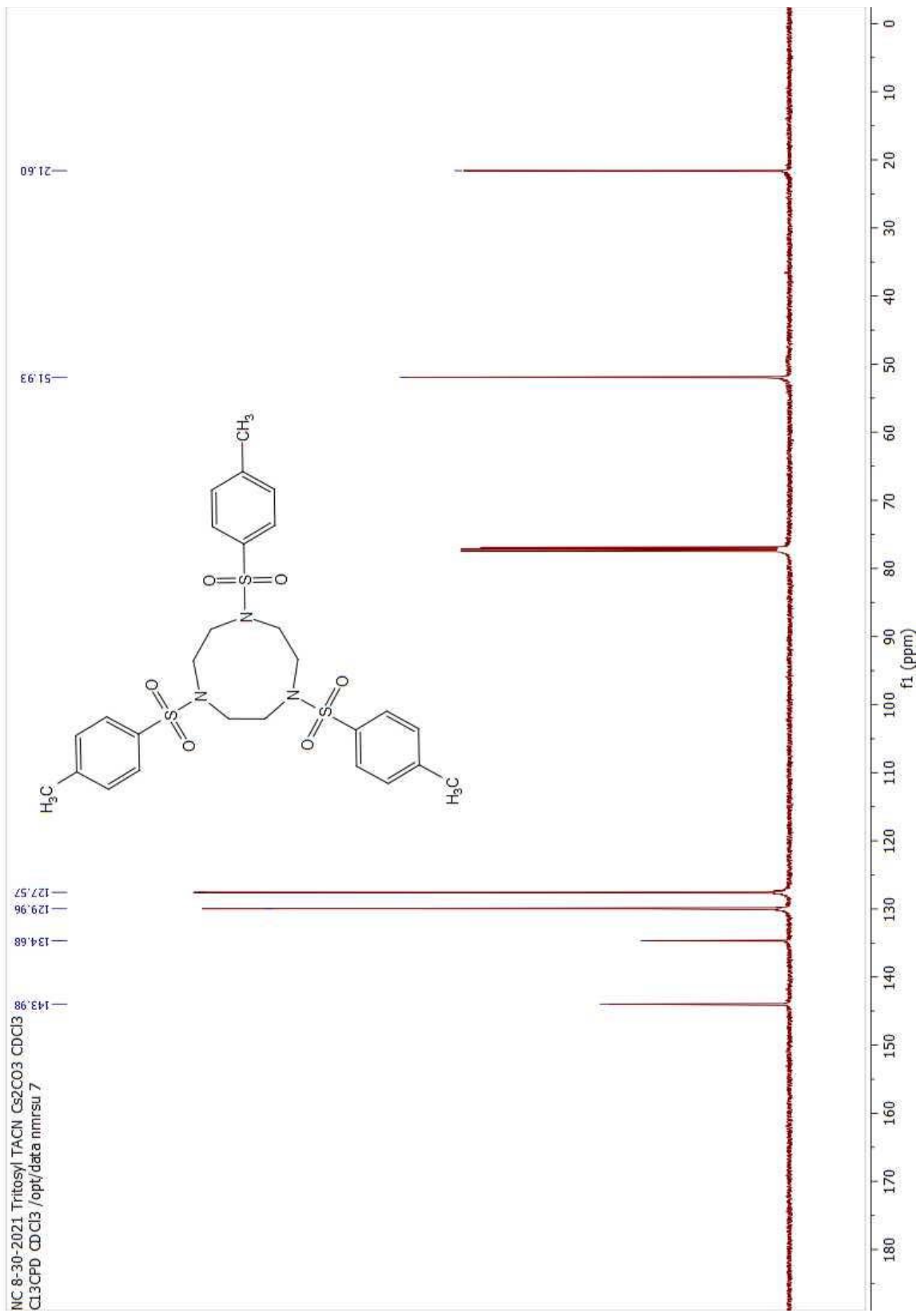


NC 8-13-21 Ditosyl Ethylene Diamine CDCl3
PROTON CDB /opt/data/nmr/su_13

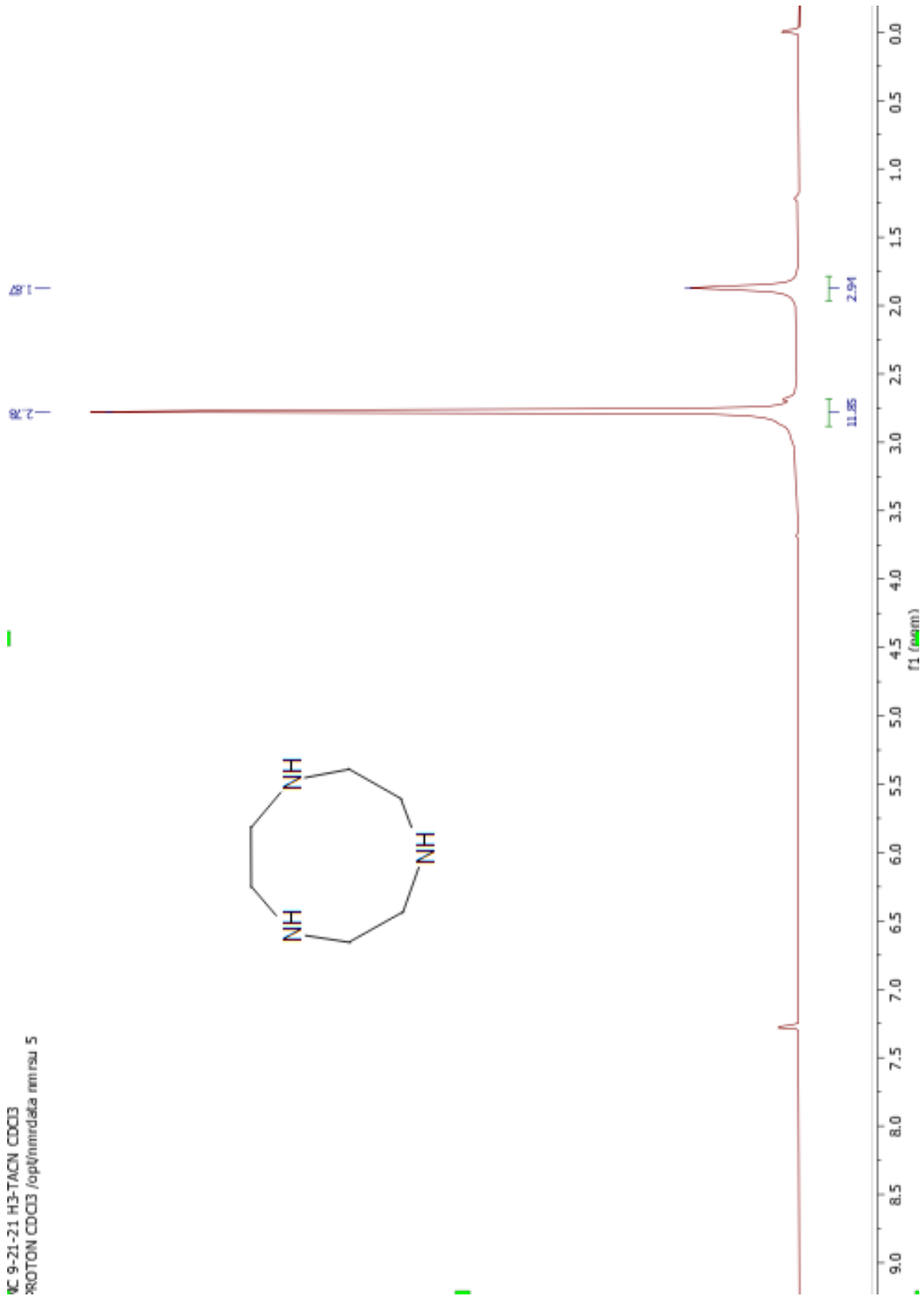


NC 8-30-2021 Tritosyl TACN Cs2CO3 CDCl3
PROTON DCB /opt/data nmrsu 7

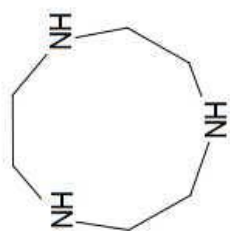




QC 9-21-21 H3-TACN CDCl3
%ROTOM CDCl3 /opt/nmrdata nmr su 5



NC 9-21-21 H3-TACN CDCl3
Cl3CPD CDCl3 /opt/nmrdata nmrsu 5



18.32



135 130 125 120 115 110 105 100 95 90 85 80 75 70 65 60 55 50 45 40 35 30 25 20 15 10 5 0
f1 (ppm)

Type	Molecule	Fragment	Classification	No. of hits	Query value	Mean	Std. dev.	Minimum	Maximum
bond	Zr(DOTPi)	Zr1 N18	Not unusual	22	2.623	2.52	0.077	2.406	2.627
bond	Zr(DOTPi)	Zr1 N25	Not unusual	22	2.623	2.52	0.077	2.406	2.627
bond	Zr(DOTPi)	Zr1 N4	Not unusual	22	2.623	2.52	0.077	2.406	2.627
bond	Zr(DOTPi)	Zr1 N11	Not unusual	22	2.623	2.52	0.077	2.406	2.627
bond	Zr(DOTPi)	P8 O3	Not unusual	17	1.499	1.501	0.015	1.473	1.522
bond	Zr(DOTPi)	C5 N4	Not unusual	74	1.487	1.493	0.024	1.371	1.583
bond	Zr(DOTPi)	C6 N4	Not unusual	74	1.494	1.493	0.024	1.371	1.583
bond	Zr(DOTPi)	C7 N4	Not unusual	16	1.5	1.491	0.017	1.459	1.518
bond	Zr(DOTPi)	C13 C5	Not unusual	11144	1.521	1.496	0.053	0.781	1.941
bond	Zr(DOTPi)	C19 C6	Not unusual	11144	1.521	1.496	0.053	0.781	1.941
bond	Zr(DOTPi)	P8 C7	Not unusual	89	1.862	1.831	0.018	1.764	1.882
bond	Zr(DOTPi)	P8 C66	Not unusual	37	1.816	1.778	0.031	1.655	1.818
bond	Zr(DOTPi)	P15 O10	Not unusual	17	1.499	1.501	0.015	1.473	1.522
bond	Zr(DOTPi)	C12 N11	Not unusual	74	1.487	1.493	0.024	1.371	1.583
bond	Zr(DOTPi)	C13 N11	Not unusual	74	1.494	1.493	0.024	1.371	1.583
bond	Zr(DOTPi)	C14 N11	Not unusual	16	1.5	1.491	0.017	1.459	1.518
bond	Zr(DOTPi)	C27 C12	Not unusual	11144	1.521	1.496	0.053	0.781	1.941
bond	Zr(DOTPi)	P15 C14	Not unusual	89	1.862	1.831	0.018	1.764	1.882
bond	Zr(DOTPi)	P15 C62	Not unusual	37	1.816	1.778	0.031	1.655	1.818
bond	Zr(DOTPi)	P22 O17	Not unusual	17	1.499	1.501	0.015	1.473	1.522
bond	Zr(DOTPi)	C19 N18	Not unusual	74	1.487	1.493	0.024	1.371	1.583
bond	Zr(DOTPi)	C20 N18	Not unusual	74	1.494	1.493	0.024	1.371	1.583
bond	Zr(DOTPi)	C21 N18	Not unusual	16	1.5	1.491	0.017	1.459	1.518
bond	Zr(DOTPi)	C26 C20	Not unusual	11144	1.521	1.496	0.053	0.781	1.941
bond	Zr(DOTPi)	P22 C21	Not unusual	89	1.862	1.831	0.018	1.764	1.882
bond	Zr(DOTPi)	P22 C58	Not unusual	37	1.816	1.778	0.031	1.655	1.818
bond	Zr(DOTPi)	P29 O24	Not unusual	17	1.499	1.501	0.015	1.473	1.522
bond	Zr(DOTPi)	C26 N25	Not unusual	74	1.487	1.493	0.024	1.371	1.583
bond	Zr(DOTPi)	C27 N25	Not unusual	74	1.494	1.493	0.024	1.371	1.583
bond	Zr(DOTPi)	C28 N25	Not unusual	16	1.5	1.491	0.017	1.459	1.518
bond	Zr(DOTPi)	P29 C28	Not unusual	89	1.862	1.831	0.018	1.764	1.882
bond	Zr(DOTPi)	P29 C52	Not unusual	37	1.816	1.778	0.031	1.655	1.818

Type	Molecule	Fragment	Classification	No. of hits	Query value	Mean	Std. dev.	Minimum	Maximum
bond	Zr[(DOTPi)(H ₂ O)]	P8 O3	Not unusual	18	1.499	1.501	0.014	1.466	1.522
bond	Zr[(DOTPi)(H ₂ O)]	C5 N4	Not unusual	16	1.485	1.484	0.048	1.376	1.605
bond	Zr[(DOTPi)(H ₂ O)]	C6 N4	Not unusual	16	1.491	1.484	0.048	1.376	1.605
bond	Zr[(DOTPi)(H ₂ O)]	C7 N4	Not unusual	16	1.493	1.491	0.017	1.459	1.518
bond	Zr[(DOTPi)(H ₂ O)]	C13 C5	Not unusual	11144	1.52	1.496	0.053	0.781	1.941
bond	Zr[(DOTPi)(H ₂ O)]	C19 C6	Not unusual	11144	1.52	1.496	0.053	0.781	1.941
bond	Zr[(DOTPi)(H ₂ O)]	P8 C7	Not unusual	86	1.856	1.831	0.019	1.764	1.882
bond	Zr[(DOTPi)(H ₂ O)]	P15 O10	Not unusual	18	1.498	1.501	0.014	1.466	1.522
bond	Zr[(DOTPi)(H ₂ O)]	C12 N11	Not unusual	16	1.486	1.484	0.048	1.376	1.605
bond	Zr[(DOTPi)(H ₂ O)]	C13 N11	Not unusual	16	1.491	1.484	0.048	1.376	1.605
bond	Zr[(DOTPi)(H ₂ O)]	C14 N11	Not unusual	16	1.494	1.491	0.017	1.459	1.518
bond	Zr[(DOTPi)(H ₂ O)]	C27 C12	Not unusual	11144	1.521	1.496	0.053	0.781	1.941
bond	Zr[(DOTPi)(H ₂ O)]	P15 C14	Not unusual	86	1.858	1.831	0.019	1.764	1.882
bond	Zr[(DOTPi)(H ₂ O)]	P22 O17	Not unusual	18	1.499	1.501	0.014	1.466	1.522
bond	Zr[(DOTPi)(H ₂ O)]	C19 N18	Not unusual	16	1.484	1.484	0.048	1.376	1.605
bond	Zr[(DOTPi)(H ₂ O)]	C20 N18	Not unusual	16	1.492	1.484	0.048	1.376	1.605
bond	Zr[(DOTPi)(H ₂ O)]	C21 N18	Not unusual	16	1.494	1.491	0.017	1.459	1.518
bond	Zr[(DOTPi)(H ₂ O)]	C26 C20	Not unusual	11144	1.52	1.496	0.053	0.781	1.941
bond	Zr[(DOTPi)(H ₂ O)]	P22 C21	Not unusual	86	1.857	1.831	0.019	1.764	1.882
bond	Zr[(DOTPi)(H ₂ O)]	P29 O24	Not unusual	18	1.498	1.501	0.014	1.466	1.522
bond	Zr[(DOTPi)(H ₂ O)]	C26 N25	Not unusual	16	1.486	1.484	0.048	1.376	1.605
bond	Zr[(DOTPi)(H ₂ O)]	C27 N25	Not unusual	16	1.492	1.484	0.048	1.376	1.605
bond	Zr[(DOTPi)(H ₂ O)]	C28 N25	Not unusual	16	1.496	1.491	0.017	1.459	1.518
bond	Zr[(DOTPi)(H ₂ O)]	P29 C28	Not unusual	86	1.86	1.831	0.019	1.764	1.882
bond	Zr[(DOTPi)(H ₂ O)]	Zr1 O70	Not unusual	1	2.519	2.261	0	2.261	2.261
bond	Zr[(DOTPi)(H ₂ O)]	P8 O2	Not unusual	16	1.577	1.524	0.019	1.49	1.56
bond	Zr[(DOTPi)(H ₂ O)]	P8 C66	Not unusual	16	1.821	1.781	0.013	1.763	1.813
bond	Zr[(DOTPi)(H ₂ O)]	P15 O9	Not unusual	16	1.575	1.524	0.019	1.49	1.56
bond	Zr[(DOTPi)(H ₂ O)]	P15 C62	Not unusual	16	1.818	1.781	0.013	1.763	1.813
bond	Zr[(DOTPi)(H ₂ O)]	P22 O16	Not unusual	16	1.578	1.524	0.019	1.49	1.56
bond	Zr[(DOTPi)(H ₂ O)]	P22 C58	Not unusual	16	1.82	1.781	0.013	1.763	1.813
bond	Zr[(DOTPi)(H ₂ O)]	P29 O23	Not unusual	16	1.578	1.524	0.019	1.49	1.56
bond	Zr[(DOTPi)(H ₂ O)]	P29 C52	Not unusual	16	1.815	1.781	0.013	1.763	1.813
bond	Zr[(DOTPi)(H ₂ O)]	Zr1 O2	Not unusual	4	2.151	2.239	0.011	2.224	2.248
bond	Zr[(DOTPi)(H ₂ O)]	Zr1 N4	Unusual	2	2.735	2.449	0.004	2.446	2.452
bond	Zr[(DOTPi)(H ₂ O)]	Zr1 O9	Not unusual	4	2.083	2.239	0.011	2.224	2.248
bond	Zr[(DOTPi)(H ₂ O)]	Zr1 N11	Unusual	2	2.722	2.449	0.004	2.446	2.452
bond	Zr[(DOTPi)(H ₂ O)]	Zr1 O16	Not unusual	4	2.147	2.239	0.011	2.224	2.248

bond	Zr[(DOTPi)(H ₂ O)]	Zr1 N18	Unusual	2	2.712	2.449	0.004	2.446	2.452
bond	Zr[(DOTPi)(H ₂ O)]	Zr1 O23	Not unusual	4	2.078	2.239	0.011	2.224	2.248
bond	Zr[(DOTPi)(H ₂ O)]	Zr1 N25	Unusual	2	2.688	2.449	0.004	2.446	2.452